Heliyon 6 (2020) e03245

Contents lists available at ScienceDirect

Heliyon

journal homepage: www.cell.com/heliyon

Review article

Synthesis, phase transformation, and morphology of hausmannite Mn_3O_4 nanoparticles: photocatalytic and antibacterial investigations

Anu Sukhdev [a,*], Malathi Challa [b,**], Lakshmi Narayani [b,c], Adalagere Somashekar Manjunatha [d], P.R. Deepthi [a], Jagadeesha V. Angadi [a], P. Mohan Kumar [a], Mehaboob Pasha [a]

[a] Material Research Centre,Presidency University, Bengaluru, 560 064, India
[b] Department of Chemistry, Ramaiah Institute of Technology, Bengaluru, 560 054, India
[c] Department of Chemistry, MES College of Arts, Commerce and Science, Bengaluru, 560 003, India
[d] Department of Chemistry, Don Bosco Institute of Technology, Bengaluru, 560 074, India

ARTICLE INFO

Keywords:
Nano hausmannite
Methods of synthesis
Morphology
Phase transformation
Photocatalyst
Antimicrobial activity
Materials science
Nanomaterials
Materials application
Materials chemistry
Materials property
Chemistry
Environmental science
Biological sciences

ABSTRACT

Nano structured Hausmannite (Mn_3O_4) has efficacious applications in numerous fields, such as catalytic, medical, biosensors, waste water remediation, energy storage devices etc. The potential application in wastewater treatment is due to its distinct structural features combined with fascinating physicochemical properties. Another area of interest is the oxidative properties imparted due to its reduction potential. Larger surface to volume ratio and high reactivity than the bulk form shows great progress as antimicrobial agent to control drug resistant microbial population. The distinct surface morphologies, crystalline forms, reaction conditions and synthetic methods exerts significant impact on the photo catalytic and bactericidal efficiency. Hence, the present paper focuses on a concise review of the multifarious study on synthetic methods of Mn_3O_4, growth mechanisms, structural forms, phase transformation and phase control, shape and dimensionality. The review also confers its applications towards photo catalytic and bactericidal studies.

1. Introduction

Numerous morphology of Mn_3O_4 have gathered benefits for their applications in sensing, ion exchange, batteries and as catalysts in its different oxidation states [1, 2, 3, 4, 5].

Unit cell of spinel structure Mn_3O_4 contains 32 oxygen and 24 cations of both di and trivalent of Mn. The fascinating physicochemical property is due to the following structural attributes: (i) oxide ions are cubic close packed (ii) Mn^{2+} occupies the tetrahedral site (iii) Mn^{3+}occupies the octahedral site (iv) d^4 state of the Mn(III) atoms in high spin configuration brings about John-Teller distortion in it. The removal efficacies of the dye pollutants in waste water by Mn (III/IV) oxides are reliant on their crystallographic systems [6, 7, 8, 9, 10]. Highest eg orbital filling due to dual valency state of Mn plays crucial role in the catalytic degradation of dyes [11].

The spawned rising interest of Mn_3O_4 as heterogeneous photo catalyst, is a prospective technology, to cut down chemical constituents and unplug pathogen cells in water [12]. The photo catalyst has to be dynamically stable as the photo catalytic reaction proceeds in an air-saturated and water-rich environment. Mn_3O_4 has fairly good thermodynamic stability in comparison with other other oxidation states. The portentous strategy to enhance the photo catalytic activity is to alter or modify morphology of nano material in different forms viz. nanotubes, nanorods, nanosheets, nanowires, nano belts, nano flower, nano coin etc.

It has also received prodigious attention as bactericidal agents and opened a new approach in encountering antibiotic resistant pathogens. This is because, materials in nano size can penetrate through nano pores of mill meter range of cell membrane and produce toxic O_2* radical to mutilate cell membranes of microbes which in turn results in an efficient restraint of microbial growth [13, 14].

* Corresponding author.
** Corresponding author.
E-mail addresses: anusukhdev@yahoo.co.in (A. Sukhdev), maalathichalla@gmail.com (M. Challa).

https://doi.org/10.1016/j.heliyon.2020.e03245
Received 22 November 2018; Received in revised form 4 May 2019; Accepted 14 January 2020

Chemical composition and synthesis methods influence the morphology and particle size distribution which are key parameters in surface area and reaction activity. Enormous synthetic methods like solvothermal, vapor phase growth, vacuum calcining precursors, thermal decomposition etc assist to tailor morphology and particle size of nano compound [15, 16].

Several researchers have reported one-dimensional Mn_3O_4 nano-materials with different morphology. As per our literature survey, various synthetic routes to achieve different morphological forms of Mn_3O_4 have been reported. There were recent reports on the exploration of micro emulsion route for the synthesis of Mn_3O_4 nano crystals to achieve belt-like morphology phase [17, 18, 19, 20, 21]. Many research groups have worked on hausmannite nano structured composites for foreseeable applications. Deepak Dubai and Rudolf Holze construed flexible birch super capacitor with Mn_3O_4 stacked nano sheets and gel electrolyte via chemical bath decomposition method [22]. Shambharkar and co-workers have synthesized polyaniline Mn_3O_4 nano composite by chemical oxidation method [23]. Karaoglu and his group coalesced PEG Mn_3O_4 nano composite via hydrothermal method and accounted for its magnetic behaviour [24]. Tamizh selvi and her team probed structural and physical properties (electrical and magnetic) of nano composites using simple sol gel route [25]. Merva group researched green chemical synthesis of Mn_3O_4 nanoparticles and its magnetic properties [26]. Harshitha and co-workers adopted a conventional and hydrothermal route to synthesize different phases viz Mn_3O_4 and Mn_2O_3 respectively using manganese chloride and hydrazine hydrate. The as synthesized Mn_3O_4 was incorporated with Chitosan and its electrochemical properties was studied [27]. Gang-Juan Lee and his group [28] reported the synthesis of Mn_3O_4 and CuO-modified zinc sulfide (ZnS) photo catalysts for visible light assisted degradation activity. Adem Kocyigit [29] fabricated the Mn_3O_4 and Mn_3O_4/Au composite thin films by spray pyrolysis technique and tested the electrical and optical behavior.

Since there are large volumes of research papers available on the synthesis of spinel manganese oxide, it is not possible to include all work in the review. Hence, selected synthetic routes which resulted in different morphology structures, phase transformations, phase control and their application towards photo catalytic and antimicrobial studies are discussed.

2. Synthesis of hausmannite

2.1. Hydrothermal method

Hydrothermal method is a simple procedure wherein controllability of size and shape of nano particles are being achieved by means of controlling the temperature and pressure of a homogenous solution taken in teflon lined stainless-steel hydrothermal reactor.

Table 1. The Effect of time on nucleation growth of nano particle [20].

Reaction time	Morphology
0 min	10–15 mm, brown colored small particles are obtained
30 min	Agglomeration of small particles
60 min	Pre octahedral shape
120 min	Octahedral shape

Yu Li [20] employed preparation of octahedron Mn_3O_4 nano compound using 0.105 g containing aqueous potassium permanganate as a precursor for manganese ions and 30 ml of polyethylene glycol (PEG200), as reducing agent which contained hydroxyl group, reduced Mn^{7+} to $Mn^{8/3}$ state. Besides, PEG 200 at low concentration behaved as a structure guiding agent to control morphology of nano compound at 100 °C, which resulted in the formation of one dimensional MnO(OH) nano rods. However, PEG at high concentration and temperature produced pseudo spherical shape nano compound. With an increase in temperature from 100 °C to 180 °C, noticeable change in the shape was observed. The influence of time on evolution of size and shape of nano Mn_3O_4 is shown in Table 1.

The anisotropic crystal growth of nano compound was obtained due to self assembly followed by ostwald ripening mechanism [20] is shown in Figure 1. Morphology and formation of the nano particle is controlled by the polymers such as PEG, (Polyethylene glycol) PAA (Poly acrylamide), PVA (Polyvinyl alcohol) etc. The polymer will function as reducing agent and shape-directing agent. In the present reaction system, concentration of the polymer and temperature, regulated morphology of nano compound.

Khalid Ahmed and co-workers [30] have found that phase transformation of manganese oxide have been occurred with variation of temperature. 0.5 mmol $KMnO_4$ was reduced by 0.2 ml formaldehyde (CH_2O) in the reaction mixture, was taken in a hydrothermal reactor and heated for 10 h at different temperatures viz.120 °C and 300 °C. At low temperature 120 °C, the precursor solution was gradually reduced to MnOOH nanorods (JCPDS:88-649) which was latter transformed to β-MnO_2 (JCPDS-24-735) at 300 °C because of dehydration of MnOOH in the existence of air. When temperature of the reaction mixture was increased at intervals of 40 °C, the morphology was changed in sequence as irregular short nano rods to mixture of nano rods and octahedron and eventually, converted to Mn_3O_4 octahedron shape by means of the accelerated reduction, nucleation growth in the reaction mixture which is shown in SEM images (Figure 2). Figure 2a and b characterizes synthesized MnO(OH) nanorods with a cross-section of 50–60 nm and length of 2–3 micro meter at 120 °C. Figure 2c represents short rod like shape at

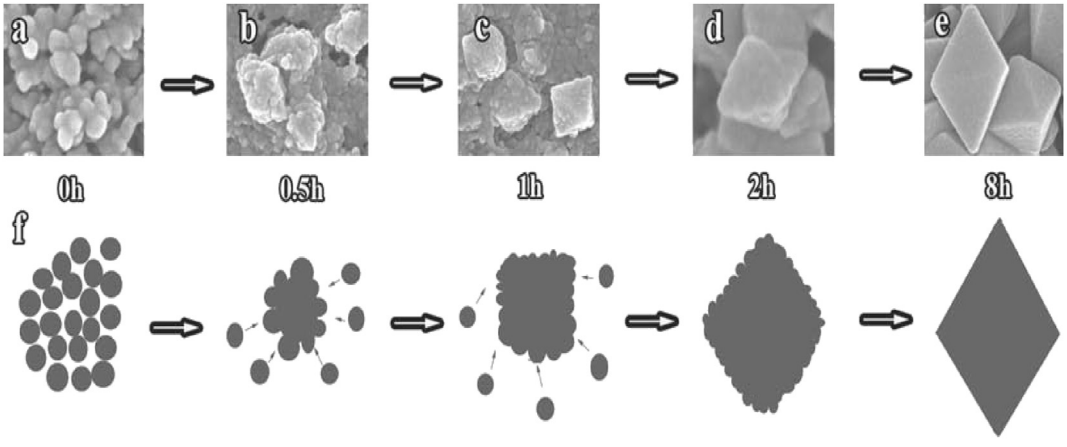

Figure 1. SEM images of the evolution process (a–e), (f) a schematic illustration of the formation of octahedral shape Mn_3O_4 nanoparticles corresponding to the SEM images. "Reprinted from Small, 7(4), Li, Y., Haiyan, T., Yang, X., Goris, B., Verbeeck,J., Bals, S., Colson, P., Cloots, R., Tendeloo, G., Su, B., 475–483., Well shaped Mn_3O_4 nano-octahedra with anomalous magnetic template and enhanced photodecomposition properties, copyright (2011), with permission from The Wiley-VCH Verlag GmbH & Co. KGaA.

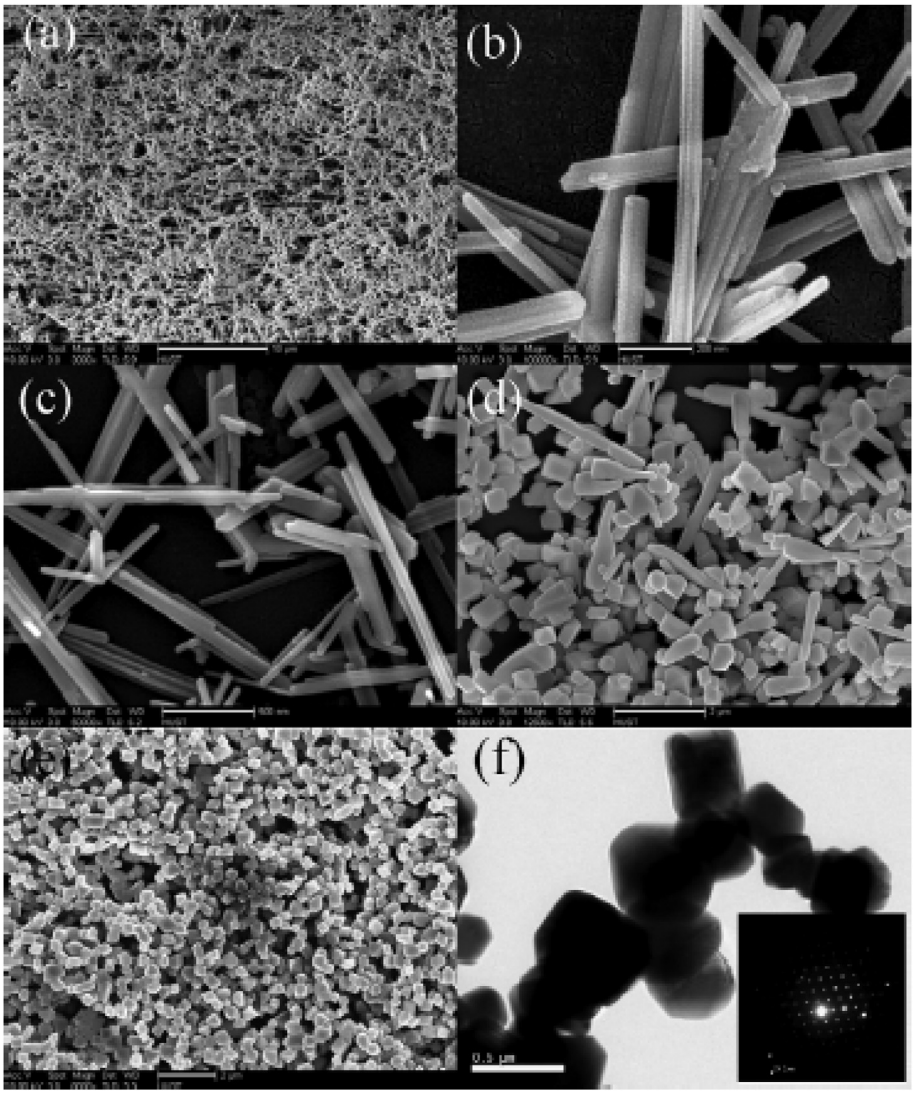

Figure 2. FE-SEM images of the synthesized sample by hydrothermal route involves conversion process from precursor nano rods to octahedron under different temperatures: (a, b) 120 °C; (c) 160 °C; (d) 180 °C; (e) 200 °C; and (f) TEM images of as-synthesized products at 200 °C. "Reprinted from Chemical Engineering Journal, 172(1), Ahmed, K. A., Peng, H., Wu, K., Huang, K., Hydrothermal preparation of nanostructured manganese oxides (MnOx) and their electrochemical and photocatalytic properties, 531-539, copyright (2011), with permission from Elsevier".

160 °C. Figure 2d represents mixture of rod and octahedron at 180 °C. At 200 °C, the as-synthesized products are octahedron-like (some have 16 faces) with edge size of 300–400 nm (Figure 2f). The transformation from precursor nanorods to octahedron is explicated in terms of Ostwald ripening process. It is alike of $BiPO_4$ and alpha Fe_2O_3 nanostructures [31, 32].

Aslam Jamal and other co-workers prepared tetragonal Mn_3O_4 (JCPDS # 024-0734), by using manganese chloride ($MnCl_2.H_2O$) as precursor for manganese ions and urea as the reducing agent with pH of 10.5 [33].

$$3MnCl_2\ (s) \rightarrow 3Mn^{2+}(aq) + 6Cl^{-}(aq) \quad (1)$$

$$NH_4OH(aq) \rightarrow NH_4^{+}(aq) + OH^{-}\ (aq) \quad (2)$$

$$3Mn^{2+} + 10OH^{-} \rightarrow 2Mn_3O_4(s) + 5H_2O + 1/2O_2 \quad (3)$$

2.2. Solvothermal method

Solvothermal synthesis allows the precise control over the size, shape distribution, and crystallinity of metal oxide nanoparticles or nanostructures.

Khaled and group [34] have adopted solvo thermal method in which tetragonal Mn_3O_4 nano belts were synthesized using coordination compound of manganese melaminate solution. The obtained nano belts matched to JCPDS # 024-0734. Diffraction peaks in XRD spectrum of sheet- like Mn_3O_4 indexing the same card number of Mn_3O_4 nanobelts and nanoparticles. The reported tetragonal phase structured Mn_3O_4 with a lattice constant of a = 5.76 A°and c = 9.47 A° and space group of I41/amd; is in good agreement with the standard data JCPDS card No. 24-0734. The characteristic diffractogram of formed sheet like Mn_3O_4 nano crystals and nano particle synthesized by solvothermal approach without melamine are corroborated [34].

$$Mn(CH_3COO)_2 + 2KOH \rightarrow Mn(OH)_2 + 2CH_3COOK \quad (4)$$

$$Mn^{2+} + nC_3N_6H_6 \rightarrow Mn\left(C_3N_6H_6\right)_2 \qquad (n = 1-4) \quad (5)$$

$$6Mn^{2+} + O_2 + 12OH^{-} \rightarrow 2Mn_3O_4 + H_2O \quad (6)$$

The concentration of melamine in the reaction mixture and reaction time had boundless impact on controlling the morphology of nano particles and its size. It functions as capping ligand. It also controls the discharge speed of Mn^{2+}ions and panels the growth direction of Mn_3O_4 nano belts [34]. It is well evidenced that the establishment of single crystalline 1D-nanobelts is through well-aligned lattice lines. The inter planar distance calculated from the lattice fringes of sample is 0.493 nm, matches to the {101} plane of tetragonal Mn_3O_4. Similar reports were cited in other works [35, 36].

In solvo thermal method, Jing Xu and co-workers [37] have found that there was no time effect on morphology of Mn_3O_4 nano particles. This was synthesized by using similar precursor for Mn and oleic acid as a reducing agent, dissolved in 100ml methanol and heated at 180 °C in different time intervals. The obtained compound was further dissolved in hexane and extracted using ethanol before subjecting it for calcination at 500 °C for 10 h while supplying air 50 ml/min in tubular furnace as to get α- Mn_2O_3 compound.

Lin He team [38] has deployed this method to get mono dispersed spherical or cubic/octahedral Mn_3O_4 nano compound. The precursor of Mn underwent to hydrolysis and condensation in presence of template pebax 2533 (polyether amide block polymers) dissolved in isopropanol. The morphology of nano compound was being influenced with variation of pebax by % of weight in the reaction mixture. High % of weight of pebax enhanced the viscosity of reaction mixture resulted in formation of spherical Mn_3O_4 nano compound. However, cubic/octahedral shaped Mn_3O_4 was obtained at low % of weight of pebax. The surface area of this Mn_3O_4 nano crystals exhibited 38.6 m^2/g larger than purchased bulk Mn_3O_4 with 3.8 m^2/g in BET test.

Developing a simple synthetic method for shape or controlling size in nano crystals is of great importance. Song Rui group [39] have used one step solvo thermal route to prepare Mn_3O_4 nanoparticles. Apparently, experiments were carried out to investigate the consequence of reaction temperature on the particle size of Mn_3O_4 NP. The difference in temperature influences the nucleation rate and thus the size of nuclei formed.

2.3. Reflux method

This is an unsophisticated, low cost approach to get abundant produce with accurate regulator over reaction factors. The control of size, morphology and crystallinity of the materials depends on the reaction time, concentration of precursors and the type of solvent employed [40].

In reflux method, Yuli Wang and group [41] have prepared Mn_3O_4, 3D-flower like structure from the refluxed homogenous solution of manganese(II)sulphate ($MnSO_4.H_2O$), urea and cetyl trimethylammonium bromide (CTAB) as surfactant which was kept under stirring at 85 °C for 24 h. It was then treated with aqueous sodium hydroxide (NaOH) solution and 30% H_2O_2 at room temperature. Further, it was washed with aqueous alcohol and dried at 400 °C for 4 h. SEM and TEM images of flower like Mn_3O_4 materials is shown in Figure 3. The morphology of 3D -flower structure of nano Mn_3O_4 was dependant on certain reaction conditions such as time, temperature and rate of addition of aq. NaOH solution. It was noticed that with altering of temperature from 50 °C to 70 °C, the morphology of nano particle changed from nano sheets to 3D hierarchical structure and with increase in reaction time, from 12h to 24 h at 85 °C produced 2D nano sheets which were eventually changed to a well shaped 3D-flower structure respectively. Apart from this, the rate of addition of aqueous NaOH solution has brought some changes in the morphology of nano compound when the solution rate was 30 drops/min, gave nano particles size of 15 nm. The flower like spherical morphology and nano rods with smooth surface having 300–500 nm length were being obtained when the addition of NaOH solution rate was 60 drops/min and 120 drops/min respectively. This modification in morphology during synthesis of nano Mn_3O_4 were due to arrangement of capping agent like shell which surrounds the precursor particles in nucleation growth, that was not disturbed by the addition of alkaline solution in slow addition whereas fast increment rate of addition of aqueous NaOH solution disturbed shell around precursor particles, which leads to form nano rods [42].

Tetragonal hausmanite was prepared by Abdulhadi Baykal et al [43] and Anil Kumar et.al from the same precursor $MnCl_2.H_2O$ mixed with aqueous NH_4OH solution adopting reflux synthetic route [44].

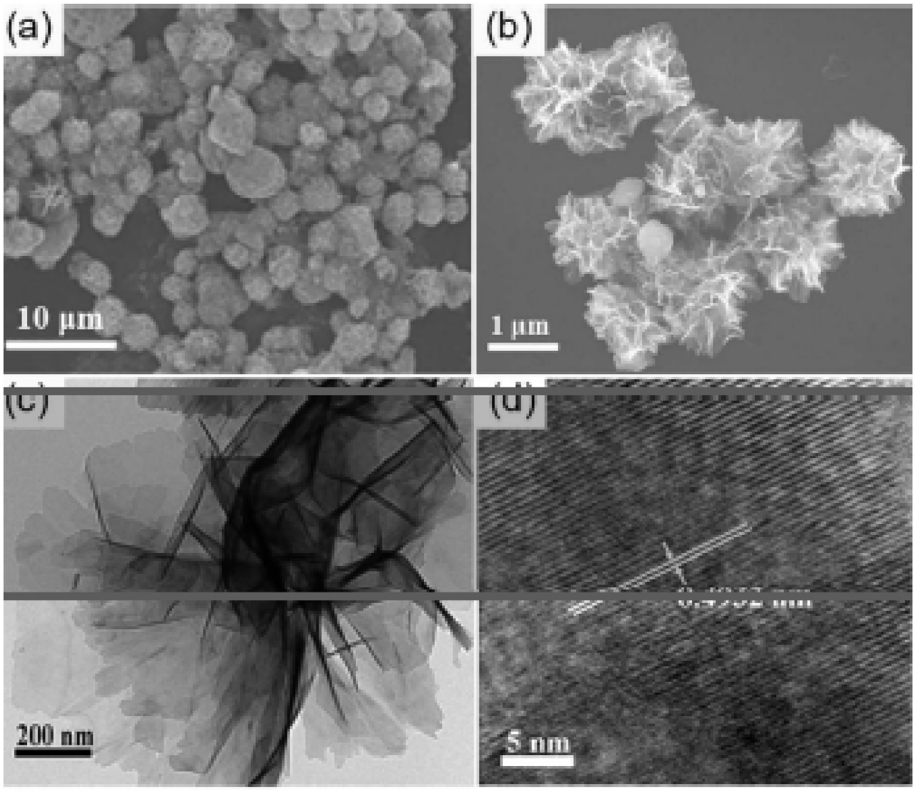

Figure 3. SEM (a and b) and TEM (c and d) images of the flower-like Mn_3O_4 nano structures. Wang, Y., Zhu, L., Yang, X., Shao, E., Deng, X., Liu, N., Wu, M., 2015, Facile synthesis of three-dimensional Mn_3O_4 hierarchical microstructures and their application in the degradation of methylene blue, J. Mater. Chem. A. 3, 2934–294 -Reproduced by permission of The Royal Society of Chemistry.

Srinivas Godavarthy and group adopted this method in which aqueous 1% tannic acid was added to 0.05 M aqueous $KMnO_4$ solution under stirring to get tetragonal Mn_3O_4 nano particle [45]. The XRD peaks of Mn_3O_4 brown precipitate coordinated to JCPDS card # 024-0734.

$$4KMnO_4 + 2H_2O \rightarrow 4MnO_2 + 4KOH + 3O_2 \quad (7)$$

$$C_7H_6O_5 + MnO_2 \rightarrow Mn(OH)_2 + C_7H_4O_5 \quad (8)$$

$$Mn(OH)_2 + O_2 \rightarrow Mn_3O_4 + H_2O \quad (9)$$

2.4. Precipitation method

The precipitation method is more economical and efficient route for mass production. The particle size depends on nucleation and growth steps which in turn depends on solution chemistry and precipitation conditions.

Hassouna Dhaouadi and co-researchers [46] have prepared Mn_3O_4 octahedron nano crystals from the homogenous mixture of $MnCl_2{\cdot}6H_2O$, aqueous NaOH solution in presence of cetyltetramethylammonium bromide (CTAB) which was put under stirring for 24 h, washed, dried in the oven at 80 °C for 24 h [47].

$$Mn^{2+} + 2OH^{-} \rightarrow Mn(OH)_2, \quad (10)$$

$$Mn(OH)_2^{-} \rightarrow MnO + H_2O \quad (11)$$

$$3MnO + 2O_2^{-} \rightarrow Mn_3O_4 \quad (12)$$

In another synthesis through precipitation method, America Vaazquez-Olmos [48] prepared tetragonal Mn_3O_4 nano rods from the immobilized colloidal solution of Mn^{2+} ions left over a period of three months. This colloidal solution was prepared using the precursor for $[Mn(CH_3COO)_2.4H_2O]$, DMF and distilled water which was sent under vigorous mixing for half an hour at room temperature. Under the present reaction conditions, the morphology of Mn_3O_4 was obtained from the crystal growth towards {001} axis devolve on the availability of Mn^{2+} ions, and crystal growth towards {101} plan, depends upon the accessibility of Mn^{3+}. UV spectrum of it showed that the peaks at 250–410 nm, 410–585 nm and 810 nm indicated transfer of charges in between $O^{2-} \rightarrow Mn^{2+}$, $O^{2-} \rightarrow Mn^{3+}$ respectively and the remaining peak at visible region of spectrum was due to d-d transitions in Mn_3O_4 nano rods.

$$Mn^{2+} + 2(OH^{-}) \rightarrow Mn(OH)_2 \quad \text{(Initiation)} \quad (13)$$

$$3Mn(OH)_2 + (1/2)O_2 \rightarrow Mn_3O_4 + 3H_2O \quad \text{(Redox – condensation process)}$$
$$\textbf{(or)}$$
$$3Mn(OAc)_2 + (1/2)O_2 -> Mn_3O_4 + 3H_2O \quad (14)$$

Spherical (coin shaped), grains and petal morphology of Mn_3O_4 was achieved through co-precipitation assisted hydro thermal, sol-gel and co-precipitation methods [49]. The growth mechanism of hausmannite depends on hydrolysis and decomposition of metallic salts. Different protocols have an effect on physical characteristics like shape, configuration, optical, magnetic and electrochemical performance of hausmannite (Mn_3O_4) The sample Mn_3O_4 synthesized by hydrothermal route retain crystalline and fine nano- petal morphology gave less resistance which displayed the intense mark on the electrochemical properties of hausmannite nanostructures [50]. The magnetic investigation revealed that the spin canting (canted movement of spin on nanoparticles) and spin slanting effect of the nano-sized particles have reduced its magnetization which is measured as coercivity (1965Oe) [51]. Therefore, the hydrothermal route could be a better method to synthesize Mn_3O_4 for super capacitor and electromagnetic applications.

There are reports that Mn_3O_4 was widely produced through several synthetic methods in which morphology and growth of Mn_3O_4 nano compounds was being controlled with the assistance of surfactant or templates [46, 52, 53].

Xinli Hao etal [54] have evaluated the effect of surfactants (CTAB, sodium oleate) and alkalies (NH_3, NaOH) in the synthesis of spherical Mn_3O_4 nano compound using simple precipitation method. In the absence of surfactants, Mn_3O_4 samples were found to be mixture of nanoparticles and particle-assembled nanosheets. This is because, the arrangement of nuclei is fast in one dimension leads to formation of nano sheets along with nano particles. On the other hand, Mn_3O_4 samples were only nanoparticles in the presence of surfactants. The formation of nano particles points the assimilation of surfactants on clusters. The concentration of OH^{-} ion plays a key factor in morphological changes from spherical to octahedral form.

2.5. Sonochemical method

Sonochemical method is a simple, low cost eco-friendly, less time consumption method. In this method, there is an interfacial region around the bubble that faced large gradients of pressure, temperature, and the rapid motion of molecules which results in the formation of excited states, bond breakage, formation of free radicals, mechanical shocks, and high shear gradients which leads to homogeneous nucleation [55, 56, 57, 58, 59]. Vahid Safarifard group have synthesized Mn_3O_4 octahedral through sono chemical method is represented in Scheme 1 [60].

Another group Shuijin Lei and co-workers [61] have developed colloidal Mn_3O_4 NP using ultra sonication in the absence of surfactant or additional nucleating factors under normal temperature and pressure. NP can also be formed without any stirring or oscillation. However, the ultrasonic pretreatment was essential to attribute the acoustic cavitation that supports Mn_3O_4 nano crystal formation. The ultrasonic waves may quicken the dispersion of Mn ions from $MnCl_2$ in ethanol amine (EA), which apparently is beneficial for the nucleation and growth of Mn_3O_4 nanocrystals.

In another simple and novel method, I.K. Gopalakrishnan group [62] has used ultrasonic irradiation method in which consequence of oxidation, reduction, dissolution and hydrolysis reactions of aqueous

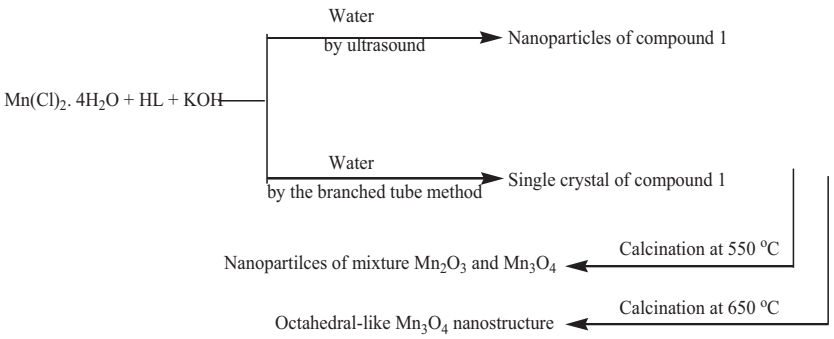

Compound 1 = $[Mn(L)_2(H_2O)2]$, (L = 1H-1,2,4-triazole-3-carboxylate)

Scheme 1. Scheme for the synthesis of Octahedral Mn_3O_4 [60].

$Mn(CH_3COO)_2.4H_2O$ (1g) solution produced, body centered tetragonal Mn3O4 nano crystallite.

$$H_2O))))) H + OH \quad (15)$$

$$H^+ + H^+ \rightarrow H_2 \quad (16)$$

$$OH^{\cdot} + OH^{\cdot} \rightarrow H_2O_2 \quad (17)$$

$$Mn(CH_3COO)_2 \rightarrow Mn^{2+} + 2(CH_3COO)_2 \quad (18)$$

$$Mn^{2+} + H_2O_2 \rightarrow Mn^{3+} \quad (19)$$

2.6. Surfactant free Mn_3O_4

Although high yields and a high crystallinity can be obtained in presence of surfactant, surfactant - free synthesis are highly desirable and appreciated as owing to absence of residual impurities on the surface of synthesized nano particles. Hence, surfactant-free synthetic routes are highly desirable [63, 64].

Zhenzhang Weng etal [65] have reported surfactant free Mn_3O_4 to oxidize toxins. Annealing Mn_3O_4 generated a porous nano-Mn_2O_3 from its integral structure that contains MnO and Mn_2O_3. The low valence Mn in oxides plays a perilous role as it readily combines with the dissolved oxygen and produces H_2O_2 which in sequence engendered hydroxyl radicals (OH•) to oxidize carbon-based pollutants without the addition of external H_2O_2, was notable in this method. It could easily be reactivated through reduction by $NaBH_4$. The authors have extended their studies on bisphenol-A by Mn_3O_4 and Mn_2O_3. The removal efficiency was found to be associated with the rise in the valence state of Mn similar to the trend observed in the phenol removal.

2.7. Ionic liquid assisted Mn_3O_4

In thermal decomposition method, Ahmad Morsali and co-workers [66] used a coordination compound, Mn (pyterpy) (H_2O) (N_3) (NO_3)) as a precursor dissolved in oleic acid, subjected to thermal decomposition at 320 °C for 2h under nitrogen atmosphere to fabricate Mn_3O_4 nano particles. Additionally, Robert Bussamara and his group [67] have prepared similar tetragonal Mn_3O_4 in controlled manner using manganese precursor and one of the ionic liquids such as 1-n-butyl-3-methylimidazoliumhexa fluoro phosphate (BMI PF6), 1-n-butyl-3-methylimidazolium tetrafluoroborate (BMI·BF4), and 1-n-butyl-3- methylimidazoliumbis(-trifluoromethanesulfonyl)imide (BMI·NTF2) dissolved in oleylamine solvent. It was noticed that Mn_3O_4 was formed only in the combination of oleylamine and BMI NTF2 solution but failed to get Mn_3O_4 nano in other two ionic solutions due to the decomposition of ionic liquid (IL). In presence of oleylamine solvent alone, the obtained Mn_3O_4 had impurity of MnO_2 indicated that ionic liquids provided a suitable medium to stabilize manganese ions in nucleation growth of nano Mn_3O_4. The study of time effect on evolution of Mn_3O_4 showed that when sample mixture of precursor, BMI·NTF2 in oleylamine was kept in the reaction at 180 °C for 96 h, produced the pure compound that had no additional peaks in XRD related to MnOOH and $Mn(CH_3COO)_2$ but it gave tetragonal Mn_3O_4 with impurities of MnOOH and $Mn(CH_3COO)_2$ when the same reaction mixture heated at180 °C for 9 h indicated that the reaction was incomplete.

Merva Gunay et al. [26] have reported the spinel-type Mn_3O_4 in the influence of ionic liquids at room temperature. Many important reactions were successfully employed using room temperature ionic liquids. The synthetic method involves addition of 0.86 g $Mn(NO_3)_2{\cdot}6H_2O$ into 2.0 g $[BMIM]BF_4$ at room temperature which was followed by drop-wise addition of 3ml of NaOH under continuous stirring. 5 mL of H_2O_2 was very slowly dropped in the mixture after about 30 min. The obtained brown precipitate was centrifuged, washed, and dried. The processing temperature plays a critical role in this method. It acted both as the reaction medium and electron transmission accelerator.

2.8. Solution combustion method

Synthesis of nano size materials by solution combustion method is adaptable, modest, low - cost and fast technique among other synthesis methods. This method comprises a self-sustained reaction in homogeneous solution of different oxidizers (e.g., metal nitrates) and fuels (e.g., urea, glycine, hydrazides). Chengjun Dong and research group [68] has adopted this route in which equi molar ratio of aqueous Mn $(NO_3)_2.4H_2O$ and ethylene glycol are subjected to combustion at 300 °C for 30 min, to produce a fluffy Mn_3O_4.

$$Mn(NO_3)_24H_2O + 6\ C_2H_6O_2 + O_2 \rightarrow 2Mn_3O_4 + 6N_2 + 12CO_2 + 42H_2O \quad (20)$$

Jagadeesh and group [69] have reported the synthesis of Mn_3O_4 nano crystallites by solution combustion method using a combination of urea and glucose fuel mixture. Increase in temperature induces phase transformation from Mn_2O_3 to Mn_3O_4. Change in temperature (Figure 4) has an effect on structural transformation and morphology. The morphological changes from spherical to rod shape suggests the anisotropic growth in samples in one direction.

2.9. Solid state method

A solid state method was employed to prepare 1D nanowire was reported by Wenzhong Wang group. They used a mixture of $MnCl_2.4H_2O$, sodium carbonate, flux NaCl and nonyl phenylether (NP-9) as a capping agent which was thermally decomposed at 850 °C for 2h. Eventually, the product was cooled to room temperature by either gradual decrease of temperature 5 °C/min or rapid decrease of temperature 40 °C/min that produced 1D nanowires of Mn_3O_4 and washed it multiple times to wipe out flux and dried it at 80 °C for 5 h. The reaction was repeated with flux and surfactant distinctly and also in absence of both under the same synthetic conditions, produced Mn_3O_4 nano particles instead of nano wires. The growth of nano wires was explained by Ostwald ripening

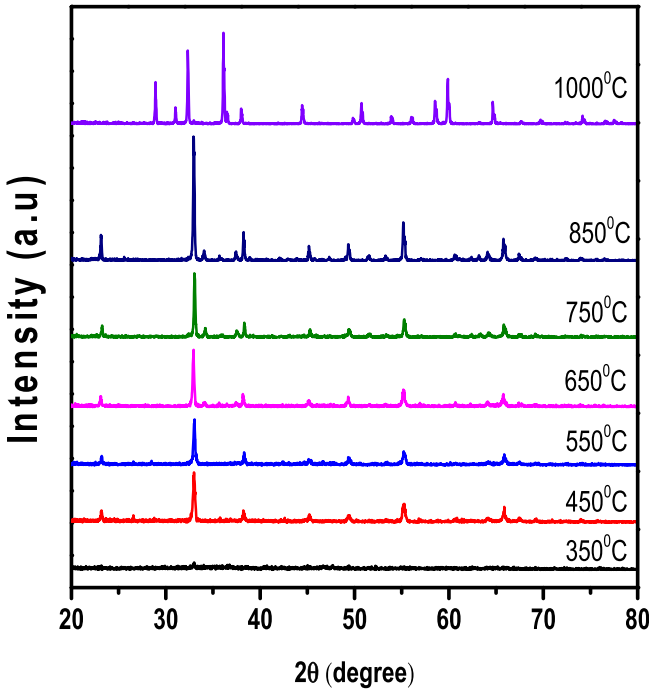

Figure 4. XRD patterns of Mn_2O_3 (350–850 °C) thermal stability of Mn_2O_3 and transition from Mn_2O_3 to Mn_3O_4."Reprinted from Journal of Magnetism and Magnetic Materials, Volume 476 (15), Lakshmi Narayani, V., Jagadeesha Angadi, Anu Sukhdev, Malathi Challa, Shidaling Matteppanavar, Deepthi, P.R., Mohan Kumar, P., Mehaboob Pasha, Mechanism of high temperature induced phase transformation and magnetic properties of Mn_3O_4 crystallites 268-273, copyright (2019), with permission from Elsevier".

mechanism was reliant on the characteristics of starting material size, chemical activity and solubility. The change in the morphology is also due to the alteration in the fluidity of the reaction mixture, mobility of the components and decrease in the eutectic temperature [70].

2.10. Green synthesis

Samaneh Ramezanpour group [71] have adopted a facile and green sol-gel method to synthesize undoped and vanadium doped Mn_3O_4 product. The characterized sample was crystallized in tetragonal Mn_3O_4 phase. It has been notified that nano rod morphology are extended with an enhance in the vanadium doping content (upto 4%). However beyond 4% addition of dopant, the particle size decrease due to accumulation. This observation proved that the doping limitation for vanadium dopant in Mn3O4 is less than 10%. Also, highest percentage of decolorization is also shown in this range.

Zehra Durmus and co-workers [72] used a green synthesis route for preparation of Mn_3O_4 nano crystals where in $Mn(NO_3)_2$.4 H_2O and an ionic liquid 1-n-butyl-3- methylimidazolium hydroxide (BMIM)OH (reaction medium and an electrical conductor for electron transfer) in aq. NaOH solution and then being treated drop wise by H_2O_2 (30w/w%, 5 ml) for 30 min. The XRD diffractogram of tetragonal Mn_3O_4 coincided with ICDD 24-0734.

$$Mn^{2+} + 2OH\text{-} \rightarrow Mn(OH)_2 \quad (21)$$

$$3Mn(OH)_2 + H_2O_2 \rightarrow Mn_3O_4 + {}_4H_2O \quad (22)$$

2.11. Other methods

Hasimur Rahaman et al. [73] reported a facile wet chemical approach for the soft-templated synthesis of Mn_3O_4 microdandelions. The superstructures of manganese oxide was synthesized using dye–surfactant in association with manganese acetate in a specific molar ratio. One of the key findings is that it has a higher BET surface area than the commercial Mn_3O_4.

Al-Nakib Chowdhary group [74] has employed forced hydrolysis method to get Mn_3O_4 nano particles by heating the precursor aq. $Mn(acetate)_2$ and further quenched in cool water. The size of Mn_3O_4 nano particles was controlled by maintaining the heating time of reaction mixture and concentration of precursor [75, 76].

E. Azhir et.al [77] employed a simple stirring method based on redox reaction between $KMnO_4$ and sodium dodecyl sulphate dissolved in aq.N_2H_4. H_2O solution leads to change the solution colour from purple to brown/black then to orange/brown which indicated the formation of nano Mn_3O_4. Finally, the product was cooled to room temperature, washed with water, ethanol and dried in vacuum. Conversely, A.K.M. Atique Ullah [78] and his group used Sol-Gel method to get tetragonal Mn_3O_4 crystallites. In this method, redox reaction took place between $KMnO_4$ solution and glycerol in the gel which was left, without disturbing for 24 h and subsequently heated at 80 °C. The XRD pattern of obtained product matched with JCPDS NO. 00-001-1127 (see Tables 2 and 3).

3. Phase transformations of manganese oxides

Manganese forms stable oxides viz. MnO, Mn_3O_4, Mn_2O_3, MnO_2, MnO(OH) as well as the metastable Mn_5O_8 can coexist or progressively change one into the other during the oxidation process. The oxidation process in the existence of manganese oxides is usually monitored by rate of oxygen diffusion. Studies have shown that formation of Mn–O phases depends on temperature, stoichiometry and composition. Phase transformation is dependant on the calcination temperature, precursors, different atmospheric gases and oxygen partial pressures [79].

LeileiLan et al [80] have prepared a selective preparation of MnOx nanostructures with crystalline phases of γ- MnOOH, β-MnO_2, α-Mn_2O_3, Mn_3O_4 in different shapes by a facile and low-temperature route. The amount of H_2O_2 or reactant concentration governs the oxidation state of manganese, crystal phases, and morphologies of MnOx nanocrystals. Bundle-like γ-MnOOH nano rods was synthesized using addition of manganese acetate, H_2O_2 and NaOH. Different phases was obtained by calcining the γ-MnOOH precursors underneath varied temperature and atmospheric environments. Further, at small reactant concentration of Manganese acetate [$Mn(CH_3COO)_2.4H_2O$] and NaOH, the γ -MnOOH is altered to α-Mn_2O_3 nano cubes whereas β-MnO_2 nanosheets were obtained by concentrating NaOH. The growth mechanism of nano wires, rods and bundle form may be in line with hydrogen bonding interface and vanderwaals forces.

G.D. Mukherjee and group [81] have reported phase changes of MnO_2, Mn_2O_3 and manganese oxide procured in sol-gel process under high pressure and temperature. Above 700 °C the sol gel Mn_3O_4 transforms to γ -Mn_2O_3. On quenching pressure from 5 GPa with a variance of 800–1200 °C temperature transmogrified [induce to a phase] to a combination of hausmannite and marokite -type structure (a mixture of Mn_3O_4 and $CaMn_2O_4$). Partial loss of crystallinity is notified in α-MnO_2 when pressure-quenched from 8 GPa at room temperature and further decomposition of α-MnO_2 increases with increase in pressure in quenching experiments.

Matthias Augustin and co-workers [82] have synthesized the time and temperature dependent phase transformations of MnOx species in oxygen and argon atmosphere. Noteworthy in this synthesis is that it is a tranquil entrée to three different nanostructured MnOx species via one calcination process which rules out synthesis caused effects. Structural and morphological studies discloses that the lattice constants and particle sizes of the MnOx species reliant on calcination temperature (see Table 4).

K.M. Atique Ullah etal [78] have reported stability of crystallites and metamorphism of Mn_3O_4 in a temperature range from 80 °C to 700 °C. Mn_5O_8 nano rods and Mn_2O_3 nano cubes were prepared by soft synthesis route by heat treatment of Mn_3O_4. The spherical Mn_3O_4 NP was converted to Mn_5O_8 rod upon heat treatment at 350 °C. This may be due to anisotropic growth mechanism. Further, double fold increase in temperature, it was observed in XRD analysis that additional peaks appeared at 750 °C, nano rods were changed to cubic Mn_2O_3 NP. In this report, morphological changes as a function of temperature shows different properties whereas the results reported by Lee et al [83] are in contrast where transmogrification of manganese oxides viz. MnO, Mn_3O_4, and Mn_5O_8 with almost identical textural properties (morphologies, surface areas, pore volumes, and the size). The structural variations and alterations of ratio of Mn and O among the various oxidation states of Mn strongly affects the properties and the strategic reason to regulate its preparation technique.

Temperature dependant phase transition [79]**:**

$$MnO \xrightarrow{190^\circ C} Mn_3O_4 \xrightarrow{430-470^\circ C} Mn_5O_8 \xrightarrow{510^\circ C} Mn_2O_3 \quad (23)$$

Phase transition using different precursors/atmospheric gases/ temperature [79]**:**

$$Mn(C_6H_4NO_2)_2 + \frac{4}{5}O_2 \overset{250^\circ C,\ air}{\rightarrow} \frac{1}{5}Mn_5O_8 + (C_5H_4N)_2 + 2CO_2 \quad (24)$$

$$Mn(C_6H_4NO_2)_2 + \frac{2}{3}O_2 \overset{370^\circ C,\ air}{\rightarrow} \frac{1}{3}Mn_3O_4 + (C_5H_4N)_2 + 2CO_2 \quad (25)$$

$$Mn(C_6H_8O_4).\ H_2O.\ Mn_3O_4 \rightarrow Mn_5O_8 \quad (26)$$

$$Mn(C_2O_4) + \frac{1}{2}O_2 \overset{300^\circ C,\ vacuum}{\rightarrow} MnO + 2CO_2 \quad (27)$$

Table 2. Synthesis routes of the Mn_3O_4 Nano compound.

Synthetic method	Reactants	Synthetic condition	Morphology/ Applications	Particle Size	Author
Hydro thermal method	0.5mmol $KmnO_4$ 0.2mlof formaldehyde	120 °C for 12 h At 200 °C for 12hr Calcination of MnOOH at 300 °C for 10 h	MnOOH nano rods Mn_3O_4 octahedron β- MnO_2 nano wires Degradation of Alizarin Yellow	50–60nm	Khalid Abdelazez Mohamed Ahmed et al.
Hydro thermal method	0.105 g or 0.005 m mol $KmnO_4$ and 30 ml PEG 200	160 °C for 12 h. Dried at 40 °C for 12 h	Octahedral shaped Mn3O4 nano particles Degradation of Rhodamine	10 nm	Yu Li et al.
Hydro thermal method	$MnCl_2$ [0.1M; 50 ml] Urea [0.1 m, 50 ml] pH -10.55 by NH_4OH	150 °C for 16 h Drying at RT	Degradation of Acridine orange Fabrication of Gold electrode Detection of alcohol	99nm	Aslam Jamala et al.
Hydrothermal method	0.7 mmol $Mn(CH_3COO)_2.4H_2O$ Melamine [1 mmol] Ethanol: water [70:30] KOH [0.08mmol]	Refluxed at 80 °C for 2 h. Autoclave heated at 200 °C for 10 h Dried in a vaccum at 50 °C for 12 h	Mn_3O_4 nano belts Mn_3O_4 nano belts	40–70 nm	Khalid Abdelazez Mohamed Ahmed et al.
Solvo thermal method	$Mn(CH_3COO)_2.4H_2O$ [14.7g] Oleic acid[8ml] Methanol[100ml]	At 180 °C Dried for 5hr in air Calcined at 400 °C for 6hr	Mn_3O_4 nano particles α Mn_2O_3	-	Jing Xu et al.
Reflux method	$MnSO_4$ .H_2O [0.19g] Urea [1.35 g] CTAB[1.2g] NaOH [2g] 30% H_2O_2 [15ml]	85 °C for 4 h Calcinations at 400 °C for 4 h	Mn_3O_4 3D flower like structure.	1-5 micro metre	Yuli Wang et al.
Reflux method	$MnCl_2.H_2O$ [0.2M] pH = 12 (NH_4OH)	At 80–100 °C for 4 h	Mn_3O_4 nano powder	50nm	M. Anilkumar et al.
Reflux method	$MnCl_2.H_2O$ [0.2M] NH_4OH	At 85 °C for 12 h	Mn_3O_4 nano particles	32nm	A. Baykal et al.
Thermal decomposition method	$MnNO_3$ [0.090g, 0.5 mmol] NaN_3 [0.065 g, 1mmol] 4'-[4-pyridyl]-2,2′6′,2′-tetrapyridine Oleic acid	Oil bath at 60 °C Dried at 186 °C Thermal decomposition of coordination compound at 320 °C	Mn_3O_4 nano particles	85nm	Ahmad Morsali et al.
Precipitation method	$MnCl_2.H_2O$ [0.22 mol] Aq NaOH [0.44 mol] CTAB[1.37 mmol]	Stirring for 24 h Dried in the oven at 80 °C for 24 h	Mn_3O_4 nano dielectric properties	20–30nm	Hassouna Dhaouadi et al.
Precipitation method	$Mn(CH_3COO)_2.4H_2O$ [0.03063g] 10% of water in DMF [22.5 ml]	Stirring 30 min And left for months	Mn_3O_4 nano rods Magnetic properties	20nm	Ameìrica Vaìzquez-Olmos et al.
Controlled synthesis	$Mn(CH_3COO)_2.4H_2O$ [0.3g] 1:24 oleylamine [7.6g] BMI-PF_6[8.18g], BMI-PF_4[6.51g]BMI-NTF_2[11.28g]	180 °Cfor 9hr in Ar atmosphere Cooled to room temperature 850 °C for 2hr	Mn_3O_4 nano particles Magnetic properties	15nm	Robert Bussamana et al.
Solid state reaction	$MnCl_2$ [0.2g] Na_2CO_3 NaCl flux [1g] NP-9 surfactant [3ml] nonylphenylether-9	Dried at 80 °C for 5hr	Mn_3O_4 nano wire Oxidation of methane and carbon monoxide Reduction of benzyl nitrate	40–80nm	Wenzhong Wang et al.
Ultra sonication method	$Mn(CH_3COO)_2.4H_2O$ (1g) in 100ml distilled water	Sonicated for 3 h and dried in a vacuum oven for few hours	Mn_3O_4 nano crystallite Magnetic property	15nm	I.K. Gopalakrishnan et al.
Reflux method	0.5 g of tannic acid in 50 ml water and mixed drop wise to 0.05 M $KmnO_4$	Stirred the contents for 5hr and then refluxed for 1hr. It is dried at 50 °C	Mn_3O_4 nano crystals Dye degradation	34nm	Srinivas Gadavarthi et al.
Combustion method	$Mn(NO_3)_2.4H_2O$ 5 mol and ethylene glycol 5 mmol	dissolved in 10 ml of distilled and combusted at 300 °C	Mn_3O_4 fluffy product Degradation of methyl orange	-	Chengjun Dong et al.
Sono chemical method.	1H-1,2,4-triazole -3-carboxylicacid (0.1 mol L_1) and potassium hydroxide (0.01 mol L_1)	Ultrasonication calcinated at 650 °C	Mn_3O_4	-	Valid Safarifard et al.

(*continued on next page*)

Table 2 (*continued*)

Synthetic method	Reactants	Synthetic condition	Morphology/ Applications	Particle Size	Author
	were added drop wise to 50 ml solution of aq. Manganese(II) chloride tetrahydrate				
Green chemical route synthesis	$Mn(NO_3)_2$.4 H_2O 2g of 1-n- butyl-3-methylimidazolium hydroxide (BMIM)OH an ionic liquid. 2M aq. NaOH solution H_2O_2 (30w/w%, 5 ml) added drop wise for 30 min		Mn_3O_4	-	Zehra Durmus et al.
Solvo thermal method	10 g with 24.2wt% of pebax 2533 in 40 mL anhydrous isopropanol (stirred at 75 °C over night 4g of $Mn(CH_3COO)_2$. 4 H_2O dissolved in 12 mL of anhydrous ethanol.	The mixture was transferred into stainless steel autoclave kept at 180 °C for 3 days to get a transparent viscous Mn_3O_4/pebax gel through hydrolysis, condensation of manganese precursor. washed with 30 ml isopropanol at 80 °C to remove pebax and vaccum dried	Mn_3O_4 spherical/ octahedral	8–32 nm	Lin He et al.
Simple stirring process	100mL 0.3 M $KmnO_4$ solution and 50 mL 0.4 M glycerol which was kept under vigorous stirring for 60 ± 10 S.	the gel was left without disturbing for 24 h and subsequently heated at 80 °C	tetragonal Mn_3O_4 crystal structure	20nm	A.K.M.Atique Ullah et al.
Simple stirring method	0.8 mmol of $KmnO_4$, 0.8 m mol sodium dodecyl sulphate dissolved in 40 ml of distilled water which was further mixed with 40 ml of 8 mmol aq.N_2H_4 . H_2O solution.	This resulted solution turned at first from purple to brown/black then to orange/brown which was stirred for 1 h at 70 °C	Mn_3O_4 crystal structure	10–30nm	E. Azhir et al.
Forced hydrolysis method	0.4 M aq. $Mn(CH_3COO)_2$. 4 H_2O was subjected to heating at 80 °C for 2 h.	The acquired product was quenched in cool water and regained by centrifugation and washed with water and dried in the oven at 40 °C.	Mn_3O_4 crystal structure Methylene blue degradation	20nm	Al-Nakib Chowdhary et al.
Sol gel method	4.6 g of manganese acetate tetrahydrate was dissolved in 30 mL of water in round bottom flask and 7.2 g of HMTA was added to the solution. In the case of Vanadium doped Mn_3O4, the desired amount of VCl_3 (2, 4 and 10% mol of VCl_3) also was added to the mixture, then the temperature set at 120 ± 2 °C for 10 h	The solution was sonicated in ultrasonic bath for 30 min then the synthesized material were collected by centrifuge, washed several times with water and dried at 90 °C for 1 h	Tetragonal Mn_3O_4 crystal structure	49–57nm	Samaneh Ramezanpour et al.

$$Mn(C_2O_4) + \frac{2}{3}O_2 \overset{370°C,\ air}{\rightarrow} \frac{1}{3}Mn_3O_4 + 2CO_2 \quad (28)$$

$$Mn^{2+} + 2OH^- \rightarrow Mn(OH)_2$$

$$3Mn(OH)_2 + H_2O_2 \rightarrow Mn_3O_4 + H_2O \quad (29)$$

4. Photo catalyst

Photo catalysis courtesy of advances in nano science is one of the most effective approaches for pollution abatement and recovery of wastewater. The photo degradation of pollutants in waste water using semiconductor nano metal oxides has been widely reported in various literature [84, 85, 86, 87]. The photo catalytic properties of metal oxide nano materials is dependent upon the following factors, namely electronic structure, desired band gap, suitable morphology, high surface area, reusability, light absorption properties and charge transport.

The general mechanism to degrade the pollutants in waste water is the generation of electrons and hole pairs from the photocatalytic semiconductor. The photo generated pair (e-/h^+) can reduce or oxidize adsorbates on the surface of the catalyst, that is shown in Figure 5 [88, 89, 90, 91, 92,100].

Table 3. Other works.

Synthetic method	Reactants	Synthetic condition	Morphology	Applications	Particle Size	Author
Mn3O4 thin films by CBD method	Manganese sulphate, hexa methylene tetramine (HMT), Polyvinyl alcohol (PVA) Stainless steel mesh number 181 with 0.09 mmwidth and 0.05 mm thickness	Well cleaned stainless steel mesh-like substrate was immersed into an aqueous solution of manganese sulfate complexed with HMT at temperature of 343 K. Brownish precipitate of Mn_3O_4 appeared in the bath. Deposition of Mn_3O_4 on substrate for 3 h Thin films were annealed at 473 K for 2 h, improve the crystallinity of deposited films.	Nano sheets	Solid state super capacitor	-	Deepak P. Dubal
Mn_3O_4/MgO nanocomposites by Sol gel	Manganese acetate and Magnesium acetate tetra hydrate 0.5 M acetic acid	mixing Mn acetate and Mg acetate solutions to get homogeneous mixture. 0.5 M of acetic acid was added drop wise with stirring maintaining temperature range 50–60 °C for 4 h. The white product obtained was dried at 90 °C for 6 h in hot air oven.	spherical	Transformer and electromagnets	-	K. Tamizh Selvi
Polyaniline–Mn_3O_4 Nanocomposite by precipitation-oxidation method	Dodecyl benzenesulphonic acid sodium salt (SDBS, 25 %), Ammonium per sulphate (NH4) 2S2O8 (APS), Manganese acetate, urea (NH2)2CO and ethylene glycol (OHCH2–CH2OH)	Aniline-SDBS (0.4 M), Mn3O4 NPs (3.72 g), $(NH4)_2S_2O_8$ (0.46 M) was Ultrasonicated 2 h; 5 °C; N_2 atmosphere. The obtained blackish green precipitate was filtered, washed and dried.	spherical	Magnetic	37–40nm	B.H. Shambharkar
Solvothermal method	0.490 g of $Mn(CH_3COO)_2$ and 15 mL of acetone	2 mmol(0.490 g) of $Mn(CH_3COO)_2$ solution and 15 mL of acetone was added in the above solution and stirred for 10 min. Then the mixture was transferred into a 25 mL stainless steel autoclave and heated at different temperatures for 12 h. The resulting product is filtered, washed and dried	spherical	supercapacitors	9–15 nm	Song Rui etal
Combustion method without fuel	$MnCl_2$ $KMnO_4$ Sodium acetate	In this method precursor $MnCl_2$ is converted to $Mn^{III}(acac)_3$ followed by calcination at 600 °C and 1000 °C to obtain Mn_3O_4 NP	spherical	Super capactiors	20–40nm	Mehdi Salehi
PEG-Mn_3O_4 nanocomposites by hydrothermal route	$Mn(acac)_2$, NH_3, PEG-400, absolute ethanol)	1 g of $Mn(acac)_2$ was added dropwise into three-neck round-bottom flask. Then 16.7ml PEG-400, heated and melted, was injected to the flask under NH_3 gas (pH = 11) with continuous stirring mixture was put in the autoclave and was kept at 160 °C for 12 h, The obtained precipitate was filtered, washed with ethanol and dried	spherical	Magnetic	12nm	Karaoglu
Mn_3O_4/graphene nanocomposites: solvothermal process	20 mg RGO 200 mL DMF 20 mL of 0.2 M $Mn(Ac)_2$.4H2O	dispersing 20 mg RGO in 200 mL DMF to 20 mL of 0.2 M $Mn(Ac)_2$. $4H_2O$ followed by sonication for 30 min and heating to 80 °C.	Spherical	Photocatalytic degradation of the MB dye	12nm	Ahmed A. Amer [72]
Mn_3O_4-Chitosan nano composites by solution casting method	1.3 g of $MnCl_2.6H_2O$ 1.3 ml of hydrazine hydrate Chitosan	Chitosan and Mn_3O_4 nano particles were dispersed through ultrasonication. The blend was solution casted in petri dish at 333K for 24 h which resulted in thin films	Thin film	Energy storage	-	B. A. Harshita,
Mn_3O_4-RGO by Sol gel method	0.6 g of graphite oxide 1.928 g of manganese acetate Tetrahydrate 10ml of hydrazine	Manganese acetate solution and GO were dispersed under vigorous magnetic stirring for 1 h. NaOH aqueous solution (50%) was added dropwise 10 mL of hydrazine hydrate was added with constant stirring at temp 80 °C for 5h Precipitate was filtered, washed and dried.	hybrid consists of disorderedly stacked graphene and crystalline Mn3O4 NPs	Dye degradation, lithium-ion batteries and supercapacitors	29 nm	Yunjin Yao [73]
Ultrasonication	0.6 g $MnCl_2$ 30 ml of ethanolamine	0.6 g $MnCl_2$ solution and 30 ml of ethanolamine were ultrasonicated for 5 h. The obtained brown precipitate was centrifuged, filtered, washed and dried	Tetragonal	magnetic	5–10 nm	Shuijin Lei

(*continued on next page*)

Table 3 (*continued*)

Synthetic method	Reactants	Synthetic condition	Morphology	Applications	Particle Size	Author
Spray Pyrolysis technique o Mn_3O_4/Au	Manganese (II) nitrate tetrahydrate and Chloroauric acid ($HAuCl_4$)	Manganese (II) nitrate tetrahydrate and Chloroauric acid ($HAuCl_4$) was stirred for one night at 70°C. Glass and Si wafer were employed as substrate for thin films. The substrates were put a hot plate which has 200°C surface temperature, and solutions were sprayed onto the substrates. The coated substrates were annealed 400°C for 1 h in the air	Thin film	sensors	18nm	Adem Kocyigit1
Manganese oxide/ bentonite nanocomposites by thermal decomposition method	10 g of Na^+–BC 4.57 g of $Mn(CH_3COO)_24H_2O$	sodium bentonite Na^+–BC (10 g) and $Mn(CH_3COO)_2$. $4H_2O$ (4.57 g) were used as starting materials, taken in molar ratio of 10:1.mixed well for 3 h to get homogenous solution.pH maintained in the range of 7–8. Obtained precipitate is centrifuged, dried and calcined at 500 °C for 5 h	Intercalation of Mn_3O_4 into bentonite clay	Antimicrobial agent	28 nm	Bama Krishnan

Non-toxicity, stability, strong oxidizing power and durability characteristics of titanium oxide have been promoted it as a hegemony among catalytic materials. The default of TiO_2 as a photo catalyst is its restricted activation under UV region and easy recombination of its electron - hole pair in visible region that impeding its photo catalytic application under visible region. Most of the semiconductor catalysts only serve under UV light which reckon for ca.4% of the total solar energy. Therefore, there is a necessity to enhance or find photo catalyst that will be activated by light of visible spectral region i. e utilizing wave length between 380 and 500 nm as to profit a maximum amount of energy available from solar radiation. In this frame work, significant efforts put together in order to improve catalytic behaviour of semiconductor oxides by modifying specific surface area and energy bad gap via anchoring of noble metals, surface defect engineering textural designing, metal and non- metal doping etc [93]. The quantum confinement in nano size compounds gives shift in optical band gap as for TiO_2 (anatase) is 3.2 eV and rutile is 3.0 eV whereas band gap of Mn_3O_4 ranges from 3.65 ev to 2.34 eV [94].

4.1. Role of manganese in improving the photo catalytic performance

Theoretical modelling demonstrated that among transition elements, manganese has intrinsic character of high optical absorption in visible and infra-red solar light. Enhancement of activity in visible region is due to tapered band gap, significant curvature and intermediate bands inside the forbidden gap [95, 96]. Deng etal [96] reported the synthesis of Mn doped TiO_2 nano crystalline powder by sol gel method. It has shown remarkable visible light photo catalytic activity in the degradation of methylene blue. The conjectural study showed that replacement of Ti by Mn ions into the TiO_2 matrix has greater photo catalytic effect due to (i) narrower band gap increased carrier mobility (ii) smaller grain size offers larger surface area (iii) inclusion of Mn into TiO_2 lattice causes intermediate bands [97, 98].

Manganese supported titania, synthesized through impregnation and sol gel method was stated by Mokhthar and group [99]. Improved photo catalytic action was observed in the mineralization of Indigo Carmine. The decrease in the proportion of –OH group was observed due to insertion of Mn in titania lattice and the rapid generation of e^-/h^+ pairs on the exterior of the catalyst designed dynamic sites. Mn/TiO_2 synthesized through impregnation method exhibits higher photo catalytic activity compared to bulk and synthesized TiO_2 in sol gel process. The influence of Mn^{3+} belongs to Mn_2O_3 in TiO_2 brings about an effective separation of charges resulting in high oxidation- reduction ability, the observed acidic hydroxyl radical and 34% of manganese coverage on the surface of Titania contributes to overall enhancement.

4.2. Comparative photocatalytic study

Manganese oxides was among the ancient observed metal oxide catalyst and originate to retain an impending action in redox reactions. The discussed photo catalytic reactions in the removal of most of the dyes have shown excellent photo catalytic activity under visible light (see Table 5).

The photocatalytic degradation of diphenyl thio carbazone (DPTC) by Mn_3O_4 was reported by Ahmed et al. [30, 34]. Catalytic performance was interpreted using UV studies. The absorbance peaks were observed at 600 and 259 nm respectively. The peak at 600 nm might be due to $n \rightarrow \pi^*$ transitions of C= N; N= N and C= S moieties in the coloured dye solution and the latter at 259 nm corresponds to $\pi \rightarrow \pi^*$ transition of aromatic ring in DPTC. The decrease in absorbance peaks indicate the degradation of dye into smaller fragments. Under the same reaction conditions, the photocatalytic efficiency has shown a remarkable improvement in the presence of oxygen and catalyst Mn_3O_4 as mixture than the individual constituents. Moreover, the morphology of Mn_3O_4 as nanobelt (NB), nanosheets (NS) and nano particles (NP) also played a role in efficiency of decomposition of dye. Mn_3O_4 nanobelt showed 99% of degradation of the dye. The improved photocatalytic activity is due to its band gap,

Table 4. Structure of Manganese oxides.

Oxide	MnO	Mn_3O_4	Mn_5O_8	α-Mn_2O_3	MnO_2	γ -MnOOH
Mineral name	Manganosite	Hausmannite		Bixbyite	Pyrolusite	Manganite
Valence	+2	+2, +3	+2,+4	3	4	3
Lattice parametersÅ	a = 4,4422	a = 5,765 c = 9,442	a = 10,347 b = 5,724 c = 4,852 β = 109,41°	a = 9,4146	a = 4,388 c = 2,865	a = 5,304 b = 5,277(1) c = 5,304(1) β = 114,38(2)°
Crystal structure	Cubic	Tetragonal	Monoclinic	Cubic	Tetragonal	Monoclinic, pseudo orthorombic

anisotropic and cubic spinel structure [10, 101]. Reactive oxygen species such as h+, $O_2^{\cdot}$ and OH^- are responsible for the photo catalytic degradation of the dye [101]. The reusability and catalytic efficiency was decreased slightly because of inescapable loss while recovery and ceasing of active centers on its surface in every cycle [30].

The kinetic and spectroscopic tools are important in understanding the catalytic behavior of the reaction. DPTC is a cationic dye which is an electron acceptor hence h + did not take part in its degradation. Hence, super oxide radicals (O^{-2}) initially took part and attacked C = S, N=N functional groups and further OH radical also involved for degradation of intermediates. The intermediates which were not stable and competing for their degradation on the same photocatalyst surface. Therefore, the equation for O^{-2} attacked initially on DPTC degradation under visible light is [100].

$$r_x = - k_6[Xads]\,[O^{-2}] \quad (30)$$

$$C_{13}H_{24}N_4S + O^{-2} \rightarrow C_{13}\,H_{23}NO + SO + NH_4 + 2NO_3 \quad (31)$$

$$C_{13}\,H_{23}NO + O^{-2} + OH \rightarrow C_7H_{12}O_2 + NO_3 + H_2O \quad (32)$$

$$C_7H_{12}O_2 + O^{-2} + OH \rightarrow CO_2 + H_2O \quad (33)$$

The comparative research on photocatalytic efficiency of MnO_x such as β-MnO_2, MnOOH nano rod and Mn_3O_4 octahedron shape on degradation of Alizarin Yellow R (AYR) [27] was carried out at different temperature, pH and time. The band gap energy of β- MnO_2, MnOOH nano rod, Mn_3O_4 were 2.14, 1.81 and 1.72 ev respectively. In accordance with L.C. Zhang et.al [102] an increase in band gap would efficiently improve charge separation of hole and e^-, results in enhanced transfer of electron at the interface of solid catalyst and dye in liquid phase, large surface area, specific capacitance and the reduction peak potential shift towards more positive which in turn leads to improved photo catalytic behavior of β-MnO_2 in degradation of AYR upto 98% compared to MnOOH nano rod and Mn_3O_4 octahedron shape [103]. The degradation mechanism of dyes was given below.

$$MnO_2 + h\nu \rightarrow \text{nano compound } (e^- + h^+) \quad (34)$$

$$e^- + O_2 \rightarrow O_2^{\cdot -} \quad (35)$$

$$O_2^{\cdot -} + H_2O \rightarrow O_2 + OH + {}^{\cdot}OH \quad (36)$$

$${}^{\cdot}OH + AYR \rightarrow \text{degradation products} \quad (37)$$

Degradation of AZY was carried out by OH radical attack at initial stage under visible light. This was confirmed by the PL studies with terephthalic acid and gradually increased peak at 427 nm with an increase in irradiation time opened that predominant oxidation reaction was of OH attack on AZY. Then,

$$r_x = {}^{-}\,k_5[Xads]\,[OH] \quad (38)$$

The intermediates formed in AZY degradation were competing their degradation on the same catalytic surface and degraded within 3 h. These intermediates were stable up to a certain period and consuming OH for their degradation.

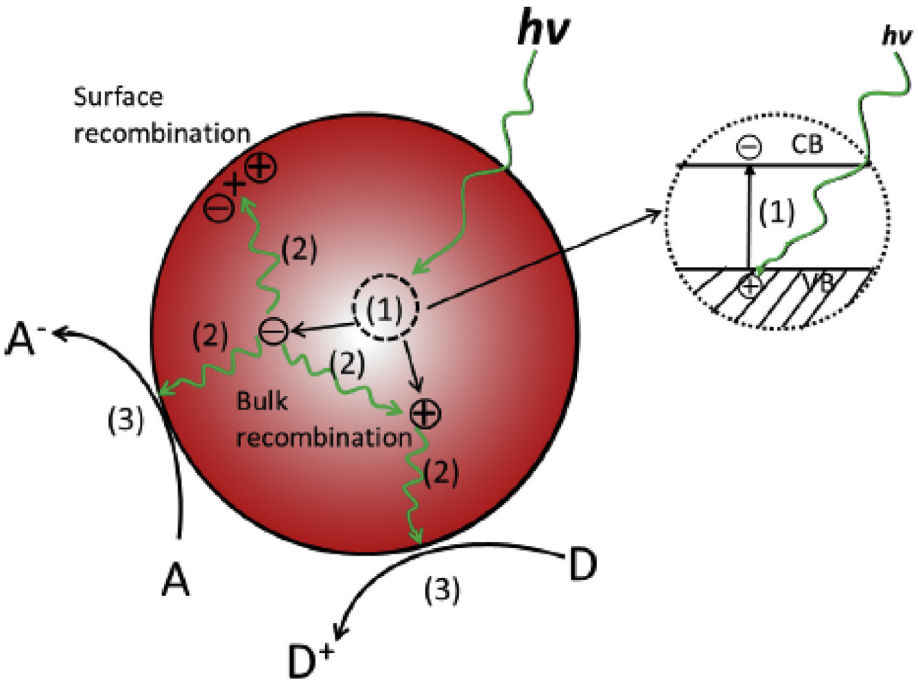

Figure 5. General mechanistic steps for the photocatalytic degradation. "Reprinted from Photochem. Photobiol. Rev, 18, Xu Zong, Lianzhou Wang, Ion-exchangeable semiconductor materials for visible light induced photocatalaysis, 32-49, copyright (2014), with permission from Elsevier".

Table 5. Dye degradation by hausmannite under different light regions.

Dye	Morphology/Band gap	Light region	Degradation %	Irradiation time	References
Acridine Orange, (AO),	Mn_3O_4 nano structures	UV-visible	47.38	170 min	Aslam Jamal et al.
Alizarin yellow	β-MnO_2, MnOOH nano rod and Mn_3O_4 octahedron(2.14, 1.81 and 1.72 ev respectively)	UV-visible	Beta MnO_2 nanowire -98% Mn3O4 octahedron -62% MnO(OH) nanorods-54%	80 min	Khalid Abdelazez Mohamed Ahmed et al.
diphenylthiocarbazone	Mn_3O_4 nanobelts, Mn_3O_4 nano sheet, Mn3O4 nanoparticles (2.22, 1.98,1.91 ev respectively)	Visible	99% Mn_3O_4 nanobelts shows higher catalytic activity than sheets and NP	150 min	Khalid Abdelazez Mohamed Ahmed
Methylene blue	Mn_3O_4 NP	visible	80%	60 min	Atique Ullah
Methylene blue	Mn_3O_4 flower structure Mn_3O_4 nano particles Mn_3O_4 nano rods	UV light	73% 49% 62%	180 min	Yuli Wang
Brilliant cresyl blue	Al_2O_3 doped Mn_3O_4 Nano wire	Visible	50–65%	300 min	Safi Asim, Bin Asif
Alizarin Red	Mn_3O_4/dandelion structure	Visible	97%	120 min	Hasimur Rahaman et al.
Methylene blue and procion red	Mn_3O_4 NP	Visible	75%	1min	Al nakhib choudhury
Malachite green	Al doped Mn_3O_4 NP	UV light	90%	60 min	Dhanasekaran et al.
Methylene blue	V doped Mn_3O_4 NP	Visible light	82.5%	40 min	Samaneh. Ramezanpour
Methyl orange	Mn3O4, hierarchical porous network	Visible light	90%	10 min	Chengjun Dong

Applying micro steady state approximation [100], it follows as

$$[OH^-] = \frac{k2[H2Oads][h+]}{k5[Xads] + \sum_i k8i\,[Yiads] + k10[M]} \quad (39)$$

A comparative study on the degradation capacity of synthesized Mn_3O_4 octahedral at 120 °C and Mn_3O_4 nano particles at 180 °C with commercial Mn_3O_4 was carried out using model pollutant Rhodamine-B (RhB) under UV light for 12h. Despite of two catalysts {Mn_3O_4 octahedral (9 $\frac{2}{m}$/g); Mn_3O_4 na no particles (7 m^2/g)} having almost the same surface area than commercial, Mn_3O_4 $_{(1}$ m^2/g), Mn_3O_4 octahedral (9 m^2/g) exhibited higher degradation capacity as 76% than the other two catalysts (45 and 23 % respectively). This enhancement of degradation capacity was due to reduction of its particle size which suppressed recombination of hole and electron resulted in transfer of electrons and holes to RhB molecules for photo decomposition. The reason being high chemical activity by Mn_3O_4 octahedral was due to larger surface energy facets than Mn_3O_4 nano particles at 180 °C and also free double bonds of Mn- or O- on the surface [104]. Commercial TiO_2 nanoparticles with <25 nm size had shown greater effect on degradation of RhB than synthesized Mn_3O_4.

The degradation efficiency of nano particle was related to its morphology and it was noticed in degradation of methylene blue (MB) in waste water treatment. Three dimensional flower like nano structure showed 73% degradation efficiency than nano particles and nano rods (49% and 62% respectively) under the given reaction conditions as UV/H_2O_2 for 3 h. The combination of nano compound and oxidizing agent without UV light showed 40% degradation of MB in waste water. The high catalytic activity of flower like structure nano compound had high surface area of 156 m^2/g, which was needed to interact with surrounding molecules of MB in degradation or adsorption process [30].

Al-Nakib Chowdhary [74] reported methylene blue, MB(30 μM) solution colour was sharply bleached out around 75% within a minute after charging 0.25 g/L of Mn_3O_4 nanoparticles suspension. Further, the colour of MB gradually disappeared at 664 nm at pH 3 and 5, respectively, with shifting of wave length towards lower side. This decolorization of MB was confirmed with cyclic voltagram (CV) in presence of sulphuric acid. The CV exhibited a well-defined redox process like anodic at 0.26 V and cathodic process at 0.21V recommended that the oxidation and reduction of MB respectively. Apart from it, the strong band at 310 nm of the procoin red (200microB) reduced almost completely by Mn_3O_4NP (0.25 g/L) suspension at pH 3 for 24 h. All these decolorisation of dyes were occurred through surface mechanism as do many other pollutants [101, 102].

In the similar manner, degradation of MB was observed by A.K.M. Atique Ullah et al. [78], when 100 mg/mL of Mn_3O_4 NP added to 100 mL of 30μM of MB in acidic medium at pH-3. Further, the spectroscopic investigation of degradation of MB showed that the degradation efficiency was 80–85% at different time intervals (from 0 min to 240 min). As time passes, the ⩽max shifted towards shorter wavelength at 628, 638, 618 and 601 nm which revealed that MB was degraded to intermediate products such as azure A, azure B, azure C and thionine respectively. The rate constant of MB degradation was 0.0045 min^{-1}. The rate constant of MB degradation was compared with akhtenskite (0.0006 min^{-1}) and birnessite (0.0007 min^{-1}). The point of zero net electrical charge (pzc) on the surface of solid phase was also determined by partially immersing it in electrolyte solution. Variation of pH plays a major role in the degradation mechanism. The pHpzc of synthesized Mn_3O_4 was 4.5. Theoretically, pH of the solution influenced catalytic performance of NP because of charge developed on catalyst surface through protonation (+ve charge on NP with lowering of pH < 4.5) and deprotonation (- ve charge on NP with increasing of pH > 4.5). However, it was observed that heterogeneous surface oxidation assisted to occur high degradation of MB while lowering pH of medium [33, 104]. This results suggested that NP was suitable for MB degradation.

Mn_3O_4 whose morphology is 3d flower like structure exhibited greater degradation of MB than TiO_2 NP [1 g/L Mn_3O_4 NP and 300 ppm dye conc,1g/LL TiO_2 NP with 20ppm dye Conc] with increase of surface area on morphological changes [105].

The degradation percentage of aq. acridine orange (AO) was improved in presence of Mn_3O_4 NP and excess oxygen rather than individually along with irradiation time [33]. There was 47% decolorization of AO achieved in presence of NP with 170 min irradiation time than simple manganese salts because of larger active and specific area of synthesized Mn_3O_4. The decolorization of methyl orange (MO) was achieved 96% within 10 min, in presence of NP, 2 mL of HNO_3 and air when it was compared to only NP catalyst (2.5%) and NP with 2 mL of HNO_3 (68%). The degradation of MO was assumed due to non-stoichiometric nature with both valencies (+3 and +2) of porous Mn_3O_4 NP lead to oxygen vacancies. This was the key issue in oxidative degradation of MO.

MO in high concentration showed 92% degradation under UV/TiO_2 NP which is due to prime factors such as particle size and band gap

energy which influenced degradation capacity of nano sized compound [106].

The degradation of methylene blue by V doped Mn_3O_4 [107] under visible light, follows the general photo catalytic mechanism. The degradation efficiency is shown better in doped Mn_3O_4 than undoped Mn_3O_4. Nano rod structure, the dopant concentration, optimum temperature and pH plays a role in the better photo catalytic activity of the semiconductor [107].

During the dye degradation of alizarin by Mn_3O_4 dandelions [73] under visible light, despite Mn_3O_4, energized dye molecule by visible light are jumped into fitted singlets and triplet states, subsequently, shifting of electron occurs from the excited dye on to conduction band CB of metal oxide forming cationic dye radicals [108]. The injected electron of Mn_3O_4 (e^-) reacts with pre-adsorbed O_2 to form oxidising species ($O2^{\cdot-}$, $HOO^{\cdot}$ followed by $^{\cdot}OH$ radicals) results in photo oxidations. Even though nano metal oxide itself is not excited, it plays a chief role in electron transfer mediation.

Developing photo catalysts that are dynamic in visible light ($\lambda \geq 420$ nm) is challenging and many alterations have been done to utilize the maximum energy from solar spectrum. One such route reported was loading nano Mn_3O_4 and CuO in ZnS photo catalyst which shifted photo absorption properties from the ultraviolet region to visible light [28]. Loading the metals onto the photo catalyst can separate photo generated electrons and holes more effectively. The photo catalytic activity was enhanced due to the effective inter particle charge transfer which prevented electron−hole recombination [73].

It has been reported that Mn_3O_4 shows greater oxidative capacity due its higher oxidation potential when compared to graphene material (rGO). Synergistic result is achieved when it is anchored [109]. Lin Duan etal have reported the significant enhancement in the oxidation of 1-napthylamine by Mn_3O_4 when it is anchored with graphene oxide. Mn_3O_4-rGO composites have shown superior degradation than the bare Mn_3O_4. The redox active surface functionalities in GO will re-oxidize the Mn(II) moiety and facilitates the oxidation mechanism of 1-napthyl amine whereas, the oxidation mechanism of 1- napthylamine by bare MnOx species, involves one electron transfer.

Recent studies [110] have shown that Graphite like carbon nitride is potential material for sunlight-driven photo catalyst. Several modifications are carried out on bare g-C_3N_4 material to improve the catalytic properties for target specific applications. One of the modification to improve is exfoliation to increase the surface area of the material.

Mario J. Muñoz-Batista and group have reported the exfoliation and deposition of Mn species in g-C_3N_4 material. Photoactivity analysis of the materials were tested under UV, visible and sunlight-type illumination for gas phase degradation of toluene. The performance is assessed by means of the quantum efficiency parameter and procedure for analysis is outlined. The simplest technique adopted for exfoliation is ultrasonication followed by surface modification using Mn species. Mn species supported in the carbon nitride materials do not show noteworthy changes in terms of the oxidation state and dispersion between the exfoliated and bulk carbon nitride samples. All structural studies carried out on the bulk, exfoliated, surface deposited samples showed physicochemical differences like in band gap energies which associated with light absorption, charge transfer and thus in photocatalytic properties. . The authors have outlined the procedure for the analysis of the true quantum efficiency parameter provides a simple route to quantitative estimate and interpret the catalytic effects originated by physical modifications of carbon nitride materials. The same can be extended to other photocatalytic materials. The highest quantum efficiency is observed in exfoliated g-C_3N_4/MnOx species under sunlight type illumination.

Yongjin Ma etal [111] have constructed a photo catalytic hetero-structure material to improve the catalytic efficiency in the visible region. Two types of hetero-junctions commonly known are: (i) Z-scheme and type-II semiconductor. They improve the separation and transportation of carriers (transferring the electrons from semiconductor A and semiconductor B) and optimal transportation path. Ma group have constructed the Mn_3O_4/CeO_2 hetero-junction by depositing Mn_3O_4 nano particle on CeO_2 nano rod surface via hydrothermal route. Mn_3O_4 is a p-type semiconductor whereas CeO_2 is a n-type. The formed n-p junction allows the fast transfer of photo-generated carriers. The photo catalytic activity is studied on the degradation of Rhodamine (RhB) in the visible region. DMPO spin-trapping ESR on Mn_3O_4/CeO_2 hetero-junction measurements explore the photo catalytic mechanism. The signals which were detected predicted the generation of O_2^- and ·OH. Species. Trapping experiments were carried out to explore the existence of holes and free radical in the photo catalytic reaction. The O_2^- and h^+ are main contributors for photo degradation and the latter one was the key contributor. Hence it can be concluded the degradation can be explained by dual mechanism. The enhanced activity might be attributed to uniformly deposited Mn_3O_4 can enlarge the visible light response range of CeO_2, which in turn improve the transfer rates of photo-excited carriers and lower their recombination rate.

5. Bactericidal agent

As bacteria have become resistant against antibiotics, treatment using metallic nano particle is the new way to fight against dangerous pathogens The size and morphology have strong influence on the bactericidal effect. The micro meter range bacterial cell contains nano size pores in its epi-cellular membranes which let to penetrate nano scale materials into bacterial cell. These nano scale materials entered into bacterial cell produces toxic oxygen radicals to mutilate cell membranes of microbes which results in an efficient control of bacterial growth [112]. Studies have shown that binding of positive charge of the metal nano particles binds with the negatively charged surface of the bacteria results in bactericidal enhancement. The bactericidal potency depends on the various factors such as the nature of the microorganisms, size of the particle, concentration, pH and morphology.

5.1. Nature of bacterial species

The sustainability or sensitivity of the bacteria against the antibacterial agents depends on the cell wall structure. Difference in cell wall structure of Gram positive and Gram negative brings some variance in their sensitivity to anti-bacterial agent. Gram positive bacteria, a denser peptidoglycan, possess a negative charge that allow to attach positive metal ions to it. On the other hand, Gram negative bacteria possess a thin negative peptidoglycan layer. This layer contains an epi membrane consisted of lipo-polysaccharide that brought structural integrity of the bacteria resulted in high immunity to antibacterial agents [112, 113, 117].

5.2. Size and shape of the particle

The size and shape of nano particles influences antibacterial activity. Decrease in particle size increases the antibacterial activity which is due to larger surface to volume ratio. Interaction of nanoparticles of various shapes with periplasmic enzymes causes different degrees of bacterial cell damage [117].

5.3. Concentration dosage

Various reports indicates that antibacterial activity increases with an increase in the dosage, but it also depends on the nature of microorganisms (gram positive and negative) [13, 117].

5.4. Effect of pH

Al Nakib etal [74] have reported the antibacterial activity carried out at pH 3.3 and 6.2. against the bacteria V. cholerae, Shigella sp., Salmonella sp., and E. coli at pH 3 and 6. Antibacterial activity of the Mn_3O_4 nanoparticle is nearly half to that of the standard ciprofloxacin antibiotic.

Moderate antibacterial activity was shown at pH 3.3 when compared to 6.2.

5.5. Procedures of assessment

Numerous bioassays like agar plug diffusion, agar well diffusion, dilution methods such as agar dilution, broth dilution are widely used to evaluate antibacterial activity in vitro. Agar disk diffusion is clinically and commonly used method to screen larger number of micro-organisms and antimicrobial agents. Since it is not possible to measure the antimicrobial agent diffused into the agar, this method is not suitable to determine the minimum inhibitory concentration (MIC) However, it offers other benefits such as plainness, inexpensive etc. Dilution methods such as agar and broth methods are more appropriate to determine MIC [13, 112, 113, 114, 115, 116, 117].

5.6. Mechanistic action of nano particles

The frequently proposed mechanistic action of metallic nano particles are (a) free metal ion toxicity arising from dissolution of the metals from surface of the nanoparticles (b) oxidative stress via the generation of reactive oxygen species (ROS) on surfaces of the nanoparticles, (c) non-oxidative mechanisms [113, 114, 115, 118, 119] which is shown in Figure 6.

Release of metal ions (NP) or generation of ROS species on the surface of the nano particles disrupts the cell wall, penetrates into the cell, damage or membrane potential modification or inhibition of t-RNA binding to ribosomes, decrease of ATP level, leakage of intracellular contents, cell differentiation, damaging vital enzymes which in turn lead to the death of bacterial cells.

5.7. Mn_3O_4 NP as antibacterial agent

The antibacterial activity of the Mn_3O_4-NPs tested against E. coli and S. aureus was reported by Azhir etal [77]. Different concentrations of Mn_3O_4-NPs using Muller Hinton Broth (MHB) medium was prepared to evaluate the minimum inhibitory concentration (MIC) and minimal bactericidal concentration (MBC). S. aureus bacterial growth was impeded around 43, 93 and 100% while for E. coli were 66, 68 and 78%, respectively. This is because S aureus is a Gram- Positive while Escherichia coli is Gram-negative and due to alteration in their structure. The antibacterial mechanism is not well documented for Mn_3O_4 NP but expected to be similar that of ZnO NP where ROS (reactive oxygen species) produced from the nano particle disrupts the cell membrane inhibiting or destroying the bacteria.

The disk diffusion method was adopted to screen the vitro antibacterial activity against (Bacillus subtilis 168) and (Escherichia coli K12) using antibiotics ampicillin (1 microgram/disk), kanamycin (1 microgram/disk), tetracycline (0.5 microgram/disk), and ciprofloxacin (1 microgram/disk) along with Mn_3O_4 NP (10 microgram/disk). Later it was incubated at 37 ^{0}Cfor 24 h. The authors [45] notified that bacterial species showed similar growth inhibition towards NP and antibiotic samples. However, it is to be noted that E. coli growth is limited by the NP's than B. subtilis.

Jayandran and group [116] have observed higher antimicrobial activity of manganese NP than the standard drug Chloramphenicol. The disc diffusion method was deployed to check antibacterial activity of manganese nano particle against gram-positive bacteria (Staphylococcus aureus and Bacillus subtilis) and gram negative bacteria (Escherichia coli and Staphylococcus bacillus), respectively and the antifungal activity against Candida albicans, Curvularia lunata, Aspergillus niger and Trichophyton simii fungi. In this comparitive study, the results of inhibition diameter clearly revealed that restrained capacity of synthesized manganese nano particles against S. aureus was extremely superior to drug.

Another group of researchers Bama Krishnan [107] et al. have established a composite material Mn_3O_4/bentonite clay (BC) and tested for bacterial strains, viz. S. aureus 25923 and P. aeruginosa 27853, and C. albicans 26790 fungus. The antimicrobial activity was tested using the well diffusion and potato dextrose agar methods. The antimicrobial activity of bentonite clay was compared with Mn_3O_4/bentonite-clay composite through inhibition diameters. The bentonite clay slowed slight activity when compared to composite. This is because ions of Mn_3O_4 are unfettered, penetration through epi and endo cytoplasmic membranes of cell wall. M. Muhamed Haneefa group [117] have synthesized a bio functional manganese oxide nanoparticles for antimicrobial activity evaluation. The synthesized nano material were bio functionalized with salicylalchitosan (SC) to enhance the antimicrobial activity. The antibacterial and the antifungal activity was evaluated by disc diffusion method and agar well diffusion method. The outcomes were matched with standard drugs namely chloramphenicol and fluconazole. Zone of inhibition data indicated the higher antimicrobial activity of bio functionalized SC/Mn_3O_4 composite than the non-functionalized NP. The reactive functional groups present in chitosan played a vital role in the boost of inhibition activity of bio functionalized nano form. Manipulation of mechanical and solubility properties enhances its antimicrobial activity.

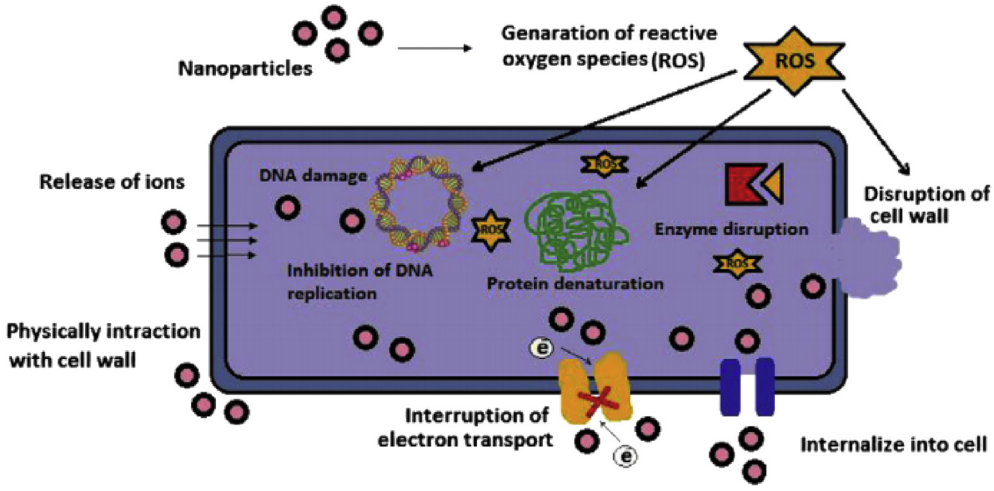

Figure 6. Various mechanisms of antimicrobial activity of the metal nanoparticles."Reprinted from Materials Science and Engineering: C, Volume 44 Solmaz Maleki Dizaj, Farzaneh Lotfipour, Mohammad Barzegar-Jalali,Mohammad Hossein Zarrintan, Khosro Adibkia, Anti-microbial activity of the metals and metal oxide nano particles. 278-284, copyright (2014), with permission from Elsevier".

6. Outlook and conclusion

Mn_3O_4 is an important oxide of manganese. As can be gleaned from the review, various synthetic protocols were discussed to prepare highly crystalline and different shapes of Mn_3O_4 nano material. Reaction time, pH, precursors and temperature has an effect on the morphology. The role of capping agent in controlling the growth and shape of NP was conferred. This review comprehends the achievements of Mn_3O_4 NP on phase control, shape, morphology, and fabrication and growth mechanism. Dynamics that promotes the phase transition and different oxides of manganese by a single synthetic procedure was exemplified. The research on photo catalytic efficiency of manganese oxide in different structural forms on dye degradation was evidenced by various research articles which makes capable and synergic photo catalyst under UV and visible light radiations. On the large scale, industries should emphasize on design and strategies for the development of active material when addressing organic contaminants in water. Strategies such as constructing heterojunctions, anchoring with graphene like materials, metal sulfide, loading globe metals, doping metal ions can be adopted to improve the photo catalytic efficiency. There is a lot of scope to make Mn_3O_4 as an effective photo catalyst by adopting different strategies in order to overcome the challenges by improving the separation efficiency of photo generated carriers, enlarge the range of photo response, and reducing the reorganization of photo generated carriers. It is an effective antimicrobial agent against various bacteria and fungus in comparison with standard antibiotic drugs. Apparently, limited work is focused on antimicrobial activity, hence adequate studies towards screening more pathogens will make Mn_3O_4 nano material as a suitable material for drug resistant pathogens and in epidermal ointments used for eczema etc.

Declarations

Author contribution statement

All authors listed have significantly contributed to the development and the writing of this article.

Funding statement

This research did not receive any specific grant from funding agencies in the public, commercial, or not-for-profit sectors.

Competing interest statement

The authors declare no conflict of interest.

Additional information

No additional information is available for this paper.

Acknowledgements

Authors thanks their management for their motivation and support.

References

[1] A.R. Armstrong, P.G. Bruce, Synthesis of layered $LiMnO_2$ as an electrode for rechargeable lithium batteries, Nature 381 (1996) 499–500.
[2] M.C. Bernard, H.L. Goff, B.V. Thi, Electrochromic reactions in manganese oxides: I. Raman analysis, J. Electrochem. Soc. 140 (1993) 3065–3070.
[3] S. Piligkos, G. Rajaraman, M. Soler Kirchner, N. Van Slageren, J. Bircher, R. Parsons, S. Gudel, H.U. Kortus, W. Wernsdorfer, G. Christou, E.K. Brechin, Studies of an enneanuclear manganese single-molecule magnet. J. Am. Chem. Soc. 127 (2005) 5572.
[4] N. Yoshikai, S.L. Zhang, K.I. Yamagata, H. Tsuji, E. Nakamura, Mechanistic study of the manganese-catalyzed [2 + 2 + 2] annulation of 1,3-dicarbonyl compounds and terminal alkynes, J. Am. Chem. Soc. 131 (2009) 4099.
[5] A.L.M. Reddy, M.M. Shaijumon, S.R. Gowda, P.M. Ajayan, Coaxial MnO_2/carbon nanotube array electrodes for high-performance lithium batteries. Nano Lett. 9 (2009) 1002.
[6] T. Subash, B. Prasad, J. Kumar, Formation and magnetic behaviour of manganese oxide nanoparticles, Mater. Sci. Eng. B 167 (2010) 153.
[7] S. Fritsch, J. Sarrias, A. Rousset, G.U. Kulkarni, Low-temperature oxidation of Mn_3O_4 hausmannite, Mater. Res. Bull. 33 (1998) 1185.
[8] S.H. Ju, D.Y. Kim, H.Y. Koo, S.K. Hong, E.B. Jo, Y.C. Kang, The characteristics of nano-sized manganese oxide particles prepared by spray pyrolysis,, J. Alloys Compd. 425 (2006) 411.
[9] Y.-F. Han, F. Chen, Z. Zhong, K. Ramesh, L. Chen, E. Widjaja, Controlled Synthesis, Characterization, and Catalytic Properties of Mn_2O_3 and Mn_3O_4 Nanoparticles Supported on Mesoporous Silica SBA-15, J. Phys. Chem. B 110 (2006) 24450.
[10] R. Tackett, G. Lawes, B.C. Melot, M. Grossman, E.S. Toberer, R. Seshadri, Magnetodielectric coupling in Mn3O4, Phys. Rev. B 76 (2007).
[11] H. He, J. Chen, Facile synthesis of monodisperse manganese oxide nanostructures and their application in water treatment, J. Phys. Chem. Chem. 112 (2008) 17540–17545.
[12] T. Koodali, Klabunde Ranjit, J. Kenneth, Nanotechnology: Fundamental Principles and Applications. A Handbook of Industrial Chemistry and Biotechnology, Springer, New York, 1973.
[13] Linlin Wang, Chen Hu, Longquan Shao, The antimicrobial activity of nanoparticles: present situation and prospects for the future, Int. J. Nano. Med. 12 (2017) 1227–1249.
[14] G.S. Thomas, | J.R. Bargar, S. Garrison, M. Bradley, Tebo, bacteriogenic manganese oxide, Accounts Chem. Res. 43 (2010) 2–9.
[15] Z.H. Wang, D.Y. Geng, Y.J. Zhang, Z.D. Zhang, Morphology, structure and magnetic properties of single-crystal Mn3O4 nanorods, J. Cryst. Growth 310 (2008) 4148–4151.
[16] N.R. Lee, H. Jung, Low-temperature fabrication of Mn3O4 nanorods by solid-state decomposition of exfoliated MnO2 nanosheets, J. Phys. Chem. Solid. 73 (2012) 1473–1477.
[17] C. Du, J. Yun, R.K. Dumas, X. Yuan, K. Liu, N.D. Browning, N. Pan, Three-dimensionally inter crossing Mn3O4 nanowires, Acta Mater. 56 (2008) 3516–3522.
[18] L. Tan, L. Meng, Q. Peng, Y. Li, One-dimensional single-crystalline Mn3O4 nanostructures with tunable length and magnetic properties of Mn3O4 nanowires, Chem. Commun. 47 (2011) 1172–1174.
[19] C. Shao, H. Guan, Y. Liu, X.X. Li, X. Yang, Preparation of Mn2O3 and Mn3O4 nanofibers via an electro spinning technique, J. Solid State Chem. 177 (2004) 2628–2631.
[20] Y. Li, T. Haiyan, X. Yang, B. Goris, J. Verbeeck, S. Bals, P. Colson, R. Cloots, G. Tendeloo, B. Su, Well shaped Mn3O4 nano-octahedra with anomalous magnetic template and enhanced photodecomposition properties, Small. Nano. Micro. 7 (4) (2011) 475–483.
[21] Y. Li, H.O. Tan, J. Lebedev, E. Verbeeck, G.V. Biermans, B.L. Tendeloo, Insight into the growth of multiple branched MnOOH nano rods, Cryst. Growth Des. 10 (2010) 2969–2976.
[22] Deepak P. Dubal, Rudolf Holze, All-solid-state flexible thin film super capacitor based on Mn3O4 stacked nano sheets with gel electrolyte, Energy 51 (2013) 407–412.
[23] B.H. Shambharkar, S.S. Umare, R.C. Rathod, Synthesis and characterization of polyaniline–Mn_3O_4 nanocomposite: electrical conductivity and magnetic studies, Trans. Indian Inst. Met. (2014).
[24] E. Karaoglu1, H. Deligoz, H. Sozeri, A. Baykal, M.S. Toprak, Hydrothermal synthesis and characterization of PEG-Mn3O4 nano composite", Nano-Micro Lett. 3 (1) (2011) 25–33.
[25] K. Tamizh Selvi, K. Alamelu Mangai, M. Priya, P. Suresh Kumar, M. Rathnakumari, Structural, electrical and magnetic properties of Mn_3O_4/MgO nano composite, J. Mater. Sci. Mater. Electron. (2010).
[26] Merva Gunay, Abdülhadi Baykal, S. Muhammet, Huseyin Sozeri Toprak, A green chemical synthesis and characterization of Mn3O4 nanoparticles, J. Supercond. Nov. Magnetism 25 (2012) 1535–1539.
[27] B.A. Harshita, D. Krishna Bhat, Aarti S. Bhatt, Synthesis of different phases of nano manganese oxides and their dielectric behaviour in chitosan composites, AIP Conf. Proc. 1391 (2011) 615–620.
[28] Gang-Juan Lee, Arumugam Manivel, Valentina Batalova, Gennady Mokrousov, Susan Masten, Jerry Wu, Mesoporous microsphere of zns photocatalysts loaded with CuO or Mn_3O_4 for the visible-light-assisted photocatalytic degradation of orange II dye, Ind. Eng. Chem. Res. 52 (2013) 11904–11912.
[29] Adem Kocyigit, Structural, optical and electrical characterization of Mn_3O_4 thin films via Au composite, Mater. Res. Express 5 (6) (2018).
[30] K.A. Ahmed, H. Peng, K. Wu, K. Huang, Hydrothermal preparation of nanostructured manganese oxides (MnOx) and their electrochemical and photocatalytic properties, Chem. Eng. J. 172 (1) (2011) 531–539.
[31] F. Xue, H. Li, Y. Zhu, S. Xiong, X. Zhang, T. Wang, X. Liang, Y. Qian, Solvothermal synthesis and photoluminescence properties of BiPO4 nano-cocoons and nanorods with different phases, J. Solid State Chem. 182 (2009) 1396–1400.
[32] H. Xu, X. Wang, L. Zhang, Zhang, Selective preparation of nanorods and micro octahedrons of Fe_2O_3 and their catalytic performances for thermal decomposition of ammonium perchlorate, Powder Technol. 185 (2008) 176–180.
[33] A. Jamal, Mohammed M. Rahman, S.B. Khan, M. Faisala, M. Abdullah, A. Aftab, A.P. Khan, A. Khan, M.N. Azum, Hydrothermally preparation and characterization of un-doped manganese oxide nanostructures: efficient photocatalysis and chemical sensing applications, Micro Nanosyst. 5 (2013) 22–28.

[34] K.A. Ahmed, K. Huang, Formation of Mn_3O_4 nanobelts through the solvothermal process and their photo catalytic property, Arab. J. Chem. (2019).

[35] Y. Ma, L. Qi, W. Shen, J. Ma, Selective synthesis of single crystalline selenium nanobelts and nanowires in micellar solutions of template surfactants, Langmuir 21 (2005) 6161–6164.

[36] Y. Zhang, G. Li, J. Zhang, J. Zhang, Shape-controlled growth of one- dimensional Sb_2O_3 nanomaterials, Nanotechnology 15 (2004) 762–765.

[37] Jing Xu, Ya-Qing Deng, Xiao-Man Zhang, Yan Luo, Wei Mao, Xue-Jing Yang, Like Ouyang, Pengfei Tian, Yi-Fan Han, Preparation, characterization and kinetic study of a core–shell Mn_3O_4@SiO_2 nanostructure catalyst for CO oxidation, ACS Catal. 4 (11) (2014) 4106–4115.

[38] He Lin, Geng Zhang, Yuanzhu Dong, Zhenwei Zhang, Shihan Xue, Xingmao Jiang, Polyether amide template synthesis of mono disperse Mn_3O_4 nanoparticles with controlled size and study of the electrochemical properties, Nano-Micro Lett. 6 (1) (2014) 38–45.

[39] S. Rui, W. Hong Jun, F. Shou-hua, Solvo thermal preparation of Mn_3O_4 particles and effect of temperature on particle size, Chem. Res. Chin. Univ. 28 (4) (2012) 577–580.

[40] H. Zhang, D. Wang, B. Yang, H. Mo, Manipulation of aqueous growth of CdTe nano crystals to fabricate colloidally stable one-dimensional nanostructures, J. Am. Chem. Soc. 128 (16) (2006) 10171–10180.

[41] Y. Wang, L. Zhu, X. Yang, E. Shao, X. Deng, N. Liu, M. Wu, Facile synthesis of three-dimensional Mn_3O_4 hierarchical microstructures and their application in the degradation of methylene blue, J. Mater. Chem. A. 3 (2015) 2934–2941.

[42] C. Chen, G. Ding, D. Zhang, Z. Jiao, M. Wu, C.H. Shek, C.M. Wu, J.K. Lai, Z. Chen, Nanoscale 4 (2012) 2590–2596.

[43] A. Baykal, Y. Köseoglu, M. Şenel, Low temperature synthesis and characterization of Mn3O4 nanoparticles, Cent. Eur. J. Chem. 5 (2007) 169–176.

[44] M. Anilkumar, V. Ravi, Synthesis of nanocrystalline Mn_3O_4 at 100˚C, Mater. Res. Bull. 40 (4) (2005) 605–609.

[45] K. Mohan Kumar, S. Godavarthi, E. Vázquez Vélez, C. Díaz, G. Syamala, Green synthesis of hausmannite nanocrystals and their photocatalytic dye degradation and antimicrobial studies, J. Sol. Gel Sci. Technol. 80 (2) (2016) 396–401.

[46] H. Dhaouadi, O. Ghodbane, F. Hosni, F. Touati, Mn_3O_4 Nanoparticles: synthesis, characterization, and dielectric properties, ISRN Spectroscopy (2012). Article ID 706398.

[47] E.R. Stobbe, B.A. De Boer, J.W. Geus, The reduction and oxidation behaviour of manganese oxides, Catal. Today 47 (1999) 161–167.

[48] A. Olmos, One-step synthesis of Mn3O4 nanoparticles: structural and magnetic study, J. Colloid Interface Sci. 29 (2005) 175–180.

[49] B. Jansi Rani, M. Ravina, G. Ravi, S. Ravichandran, V. Ganesh, R. Yuvva kumar, Synthesis and characterization of hausmannite (Mn_3O_4) nano structures, Surface. Interfac. 11 (2018) 28–36.

[50] J.S. Sherin, J.K. Thomas, J. Suthagar, Combustion synthesis and magnetic studies of hausmannite Mn_3O_4 nanoparticles, Int. J. Eng. Res. Dev. 10 (2014) 34–41.

[51] Y. Tian, D. Li, J. Liu, H. Wang, J. Zhang, Y. Zheng, T. Liu, S. Hou, Facile synthesis of Mn_3O_4 nanoplates-anchored graphene microspheres and their applications for supercapacitors, Electrochim. Acta 257 (2017) 155–164.

[52] Q. Zhang, Y. Liu, Y. Duan, N. Fu, Q. Liu, Y. Fang, Q. Sun, Y. Lin, Mn_3O_4/template composite as counter electrode in dye sensitized solar, RSC Adv. 4 (2014) 15091–15097.

[53] Lu Wang, Lin Chen, Yuhong Li, Hongmei Ji, Gang Yang, Preparation of Mn_3O_4 nanoparticles at room condition for super capacitor application, Powder Technol. 235 (2013) 76–81.

[54] Xinli Hao, Jingzhe Zhao, Yuehong Song, Zhifang Huang, Synthesis and oxidizability study on Mn_3O_4 nanoparticles, J. Nano Res. 48 (2017) 138–147.

[55] W.J. Son, J. Kim, W.S. Ahn, Sonochemical synthesis of MO5, Chem. Commun. (2008) 6336–6338.

[56] L.G. Qiu, Z.Q. Wu, Y. Wang, W. Xu, X. Jiang, Facile synthesis of nano crystals of a micro porous metal-organic framework by an ultrasonic method and selective sensing of organo amines, Chem. Commun. (2008) 3642–3644.

[57] M.A. Alavi, A. Morsali, Synthesis and characterization of Mg (OH) $_2$ and MgO nanostructures by ultrasonic method, Ultrason. zz. 17 (2010) 441–446.

[58] A. Aslani, A. Morsali, Sonochemical synthesis of nano-sized metal-Organic lead (II) polymer: a precursor for the preparation of nano-structured lead (II) iodide and lead (II) oxide, Inorg. Chim. Acta. 362 (2009) 5012–5016.

[59] V. Safarifard, A. Morsali, Sonochemical syntheses of a nanoparticles cadmium (II) supramolecule as a precursor for the synthesis of cadmium (II) oxide nanoparticles, Ultrason. Sonochem. 19 (2012) 1227–1233.

[60] V. Safarifard, A. Morsali, Sonochemical syntheses of a new fibrous-like nano-scale manganese (II) coordination supramolecular compound; precursor for the fabrication of octahedral-like Mn3O4 nano-structure, Ultra, Sonochem 21 (2014) 253–261.

[61] S. Lei, K. Tang, Z. Fang, H. Zheng, Ultrasonic assisted synthesis of colloidal Mn3O4 nano particles at normal temperature and pressure, Cryst. Growth. Des. 6 (2006) 1757–1760.

[62] I.K. Gopalakrishnan, N. Bagkar, R. Ganguly, S.K. Kulshreshtha, Synthesis super paramagnetic Mn_3O4 nano crystallites by ultrasonic irradiation, J. Cryst. Growth 280 (2005) 436–441.

[63] Moritz Wolf, Nico Fischer, Michael Claeys, Surfactant-free synthesis of monodisperse cobalt oxide nanoparticles of tunable size and oxidation state developed by factorial design, Mater. Chem. Phys. (2018).

[64] Z. Wan, J.L. Wang, Degradation of sulfamethazine antibiotics using Fe_3O_4-Mn_3O_4 nano composite as a Fenton-like catalyst, J. Chem. Technol. Biotechnol. (2016).

[65] Z. Weng, J. Li, Y. Weng, M. Feng, Z. Zhuang, Y. Yu, Surfactant-free porous nano-Mn_3O_4 as a recyclable Fenton-like reagent that can rapidly scavenge phenolics without H_2O_2, J. Mater. Chem. A A 5 (30) (2017) 15650–15660.

[66] A. Morsali, H. Hossieni Monfared, Morsali, Synthesis and characterization of Mn3O4 nanoparticles via thermal decomposition of a new synthesized hydrogen bonded polymer, J. Mol. Struct. 938 (2009) 10–14.

[67] Roberta Bussamara, Wellington W. Melo, Jackson D. Scholten, P. Migowski, Graciane Marin, Maximiliano J. Zapata, G. Machado, R.T. Sérgio, M.A. Novak, J. Dupont, Controlled synthesis of Mn_3O_4 nanoparticles in ionic liquids, Dalton Trans. 42 (2013) 14473–144778.

[68] Chengjun Dong, Xu Liu, Hongtao Guan, Xuechun Xiao, Yude Wang, Combustion synthesized hierarchically porous Mn3O4 for catalytic degradation of methyl orange, Can. J. Chem. Eng. 95 (4) (2017) 643–647.

[69] V. Lakshmi Narayani, Jagadeesha Angadi, Anu Sukhdev, Malathi Challa, Shidaling Matteppanavar, P.R. Deepthi, P. Mohan Kumar, Mehaboob Pasha, Mechanism of high temperature induced phase transformation and magnetic properties of Mn_3O_4 crystallites, J. Magn. Magn Mater. 476 (15) (2019) 268–273.

[70] W.Z. Wang, C.K. Xu, G.H. Wang, Y.K. Liu, C.L. Zheng, Preparation of smooth single-crystal, Mn_3O_4 nanowires, Adv. Mater. 14 (11) (2002) 837–840.

[71] S. Ramezanpour, I. Sheikhshoaie, M. Khatamian, Synthesis, characterization and photo catalytic properties of V doped Mn_3O_4 nanoparticles as a visible light-activated photo catalyst, J. Mol. Liq. 231 (2017).

[72] D. Zehra, K. Hüseyin, B. Abdulhadi, M.S. Toprak, A green chemical route for the synthesis of Mn_3O_4 nanoparticles, Cent. Eur. J. Chem. 7 (3) (2009) 555–559.

[73] R. Hasimur, G. Sujit Kumar, Soft-template synthesis of Mn_3O_4 micro dandelions for the degradation of alizarin red under visible light Irradiation, RSC Adv. 6 (2016) 4531–4538.

[74] Al-Nakib Chowdhury, M. Shafiul Azam, M. Aktaruzzaman, Abdur Rahim, Oxidative and antibacterial activity of Mn_3O_4, J. Hazard Mater. 172 (2009) 1229–1235.

[75] M. Ocana, Uniform particles of manganese compounds obtained by forced hydrolysis of manganese (II) acetate, Colloid Polym. Sci. 278 (2000) 443–449.

[76] Z.W. Chen, J.K. Lai, C.H. Shek, Shape-controlled synthesis and nano structure evolution of single crystal Mn_3O_4, Scripta Mater. 55 (8) (2006) 735–738.

[77] E. Azhira, R. Etefagh, N. Shahtahmasebia, M. Mashreghi, P. Pordeli, Preparation, characterization and antibacterial activity of manganese oxide Nanoparticles, Phys. Chem. Res. 3 (3) (2015) 197–204.

[78] A.K.M. Ullah, K. Kibria Akter, Firoz Tareq, Oxidative degradation of methylene blue using Mn_3O_4 nanoparticles, Water Cons. Sci. Eng. 1 (4) (2017) 249–256.

[79] Susana G. Sanfélix, Manganese Oxide Nanoparticles: Synthesis and Magnetic Properties, Technical Report, 2008.

[80] L. Leilei, G. Guangrui, L. Quanjun, Z. Huafang, K. Xu, B. Liu, L. Bingbing, Manganese oxide nanostructures: low-temperature selective synthesis and thermal conversion, RSC Adv. 5 (2015) 25250.

[81] G.D. Mukherjee, S.N. Vaidya, C. Karunakaran, High pressure and high temperature studies on manganese oxides, Phase Transitions 75 (6) (2002) 557–566.

[82] M. Augustin, D. Fenske, I. Bardenhagen, A. Westphal, M. Knipper, T. Plaggenborg, J. Kolny Olesiak, J. Parisi, Manganese oxide phases and morphologies: a study on calcination temperature and atmospheric dependence, Beilstein J. Nanotechnol. 6 (2015) 47–59.

[83] J.H. Lee, Y.J. Sa, T.K. Kim, H.R. Moon, S.H. Joo, A transformative route to nanoporous manganese oxides of controlled oxidation states with identical textural properties, J. Mater. Chem. A. 2 (2014) 10435–10443.

[84] E. Pelizzetti, C. Minero, Metal oxides as photo catalysts for environmental detoxification comments, Inorg. Chem. 15 (1994) 297–337.

[85] T. Hisatomi, J. Kubota, K. Domen, Recent advances in semiconductors for photo catalytic and photo electrochemical water splitting, Chem. Soc. Rev. 43 (2014) 7520–7535.

[86] M.R. Hoffmann, S.T. Martin, W. Choi, D.W. Bahnemann, Environmental applications of semiconductor photo catalysis, Chem. Rev. 95 (1995) 69–96.

[87] A. Hernandez-Ramırez, I. Medina-Ramırez, Photo Catalytic Semiconductors-Synthesis, Characterization, and Environmental Applications, Springer, 2015.

[88] M.G. Neelavannan, C.A. Basha, Electrochemical-assisted photocatalytic degradation of textile wash water, Separ. Purif. Technol. 61 (2008) 168–174.

[89] B. Padhi, Pollution due to synthetic dyes toxicity & carcinogenicity studies and remediation, Int. J. Environ. Sci. 3 (2012) 940–955.

[90] Zong Xu, Lianzhou Wang, Ion-exchangeable semiconductor materials for visible light induced photocatalaysis, Photochem. Photobiol. Rev. 18 (2014) (2014) 32–49.

[91] Hongjun Chen, Lianzhou Wang, Nanostructure sensitization of transition metal oxides for visible-light photocatalysis, Beilstein J. Nanotechnol. 5 (2014) 696–710.

[92] K. Okitsu, K. Iwasaki, Y. Yobiko, H. Bandow, R. Nishimura, Y. Maeda, Sonochemical degradation of azo dyes in aqueous solution: a new heterogeneous kinetics model taking into account the local concentration of OH radicals and azo dyes, Ultrason. Sonochem. 12 (2005) 255–262.

[93] A. Masakazu, T. Masato, Design and development of second-generation titanium oxide photo catalysts to better our environment—approaches in realizing the use of visible light, Int. J. Photoenergy 3 (2001) 89–94.

[94] R.N. Bhargava, D. Gallagher, X. Hong, A. Nurmikko, Optical properties of manganese-doped nano crystals of ZnS, Phys. Rev. Lett. 72 (1994) 416.

[95] H. Nasser Mohammed, A. Dahshan, Facile synthesis and optical band gap calculation of Mn_3O_4 nanoparticles, Mater. Chem. Phys. 137 (2012) 637e643.

[96] Q.R. Deng, X.H. Xia, M.L. Guo, Y. Gao, G. Shao, Mn-doped TiO_2 nano powders with remarkable visible light photo catalytic activity, Mater. Lett. 65 (2011) 2051–2054.
[97] G. Shao, Electronic structures of manganese-doped rutile TiO_2 from first principles, J. Phys. Chem. C 112 (2008) 18677–18685.
[98] G. Shao, Red shift in manganese- and iron-doped TiO_2: a DFT+U analysis, J. Phys. Chem. C 113 (2009) 6800.
[99] M. Mohamed Mokhtar, I. Othmanb, R.M. Mohamed, Synthesis and characterization of MnOx/TiO_2 nanoparticles for photo catalytic oxidation of indigo carmine dye, J. Photochem. Photobiol. A: Chemistry 191 (2007) 153–161.
[100] M.J. Munoz-Batista, M.M. Ballari, A. Kubacka, O.M. Alfana, M. Fernandex-Garcia, Braiding kinetics and spectroscopy in photo-catalysis: the spectro-kinetic approach, Chem. Soc. Rev. 48 (2019) 637–682.
[101] M.E.A. Raj, G.S. Victoria, J.V. Bena, C. Ravidhas, J. Wollschler, M. Suendorf, M. Neumann, M. Jayachandran, C. Sanjeeviraja, XRD and XPS characterization of mixed valence Mn_3O_4 hausmannite thin films prepared by chemical spray pyrolysis, technique, Appl. Surf. Sci. 256 (2010) 2920–2926.
[102] L.C. Zhang, Q. Zhou, Z.H. Liu, X.D. Hou, Y.B. Li, Y. Lv, Novel Mn_3O_4 microoctahedra: promising cataluminescence sensing material for acetone, Chem. Mater. 21 (2009) 5066–5071.
[103] L. Kumaresan, M. Mahalakshmi, M. Palanichamy, V. Murugesan, Synthesis, characterization and photo catalytic activity of Sr^{2+} doped TiO_2 nano plates, Ind. Eng. Chem. Res. 49 (2010) 1480–1485.
[104] Xinli Hao, Jingzh Zhao, Yan Zhao, Dechong Ma, Yan Lu, Jingnan Guo, Zeng Qi, Mild aqueous synthesis of urchin-like MnOx hollow nanostructures and their properties for RhB degradation, Chem. Eng. J. 229 (2013) 134–143.
[105] R.S. Dariania, A. Esmaeilia, A. Mortezaalia, S. Dehghanpour, Photo catalytic reaction and degradation of methylene blue on TiO2nano-sized particles, Optik 127 (2016) 7143–7154.
[106] Dessy Ariyanti, Mathilde Maillot, Wei Gao, TiO_2 used as photo catalyst for rhodamine B degradation under solar radiation, Int. J. Mod. Phys. B 31 (2017) 1744095.
[107] Bama Krishnan, Sundrarajan Mahalingam, Facile synthesis and antimicrobial activity of manganese oxide/bentonite nano composites, Res. Chem. Intermed. 43 (4) (2017) 2351–2365.
[108] Y. Liu, J. Hu, C. Ngo, S. Prikhodko, S. Kodambaka, J. Li, R. Richards, Gram-scale wet chemical synthesis of Wurtzite-8H, nano porous ZnS spheres with high photo catalytic activity, Appl. Catal., B 106 (2011) 212–218.
[109] Lin Duan, Zhongyuan Wang, Yan Hou, Zepeng Wang, Guandao Gao, Wei Chen, J. Pedro, J. Alvarez, The oxidation capacity of Mn_3O_4 nanoparticles is significantly enhanced by anchoring them onto reduced graphene oxide to facilitate regeneration of surface-associated Mn(III), Water Res. 103 (2016) 301–308.
[110] Mario J. Munoz-Batista, Olga Fontelles-Carceller, Kubacka Anna, Marcos Fernández-García, Effect of exfoliation and surface deposition of MnOx species in g-C_3N_4: toluene photo-degradation under UV and Visible light, Appl. Catal. B Environ. (2016).
[111] Yongjin Ma, Jing Jiang, Anquan Zhu, Pengfei Tan, Bian Yuan, Weixuan Zeng, Hao Cui, Jun Pan, Enhanced visible light photo catalytic degradation by Mn_3O_4/CeO_2 heterojunction: a Z-scheme system photo catalyst, Inorg. Chem. Front 5 (2018) 2579–2586.
[112] G. Apperlot, A. Lipovsky, R. Dror, N. Perkas, Y. Nitzan, R. Lubart, Enhanced antibacterial activity of nano crystalline ZnO due to increased ROS-mediated cell injury, Adv. Funct. Mater. 19 (2009) 842–852.
[113] A. Sirelkhalim, S. Mahmud, A. Seeni, N.H.M. Kaus, L.C. Ann, S.K.M. Bakhori, Review on Zinc oxide nano particles: antibacterial activity and toxicity mechanism, Nano-Micro Lett. 7 (2015) 219–242.
[114] M.J. Hajipur, K.M. Fromm, A.A. Ashkarran, D.J. de Aberasturi, I.R. deLarramendi, T. Rojo, Antibacterial properties of nano particles, Trends Biotechnol. 30 (2012) 499–511.
[115] C. Baker, A. Pradhan, L. Pakstis, D.J. Pocchan, S.I. Shah, Synthesis and antibacterial properties of silver nano particles, J. Nanosci. Nanotechnol. 5 (2005) 244–249.
[116] M. Jayandran, M. Muhamed Haneefa, V. Balasubramanian, Green synthesis and characterization of Manganese nanoparticles using natural plant extracts and its evaluation of antimicrobial activity, J. Appl. Pharmaceut. Sci. 5 (12) (2015) 105–110.
[117] M. Muhamed Haneefa, M. Jayandran, V. Balasubramanian, Green synthesis characterization and antimicrobial activity evaluation of manganese oxide nanoparticles and comparative studies with salicylalchitosan functionalized nano form, Asian J. Pharm. 11 (1) (2017) 65–70.
[118] S.M. Dizaj, F. Loftifur, M.B. Jalali, M.H. Jarrintan, K. Adibkia, Anti-microbial activity of the metals and metal oxide nano particles, Mater. Sci. Eng. C 44 (2014) 278–284.
[119] X. Zong, L. Wang, Ion-exchangeable semiconductor materials for visible light-induced photocatalysis, J. Photochem. Photobiol. C: Photochem. Rev. 18 (2014) 32–49.